nature portfolio

https://doi.org/10.1038/s41586-026-10864-2

Supplementary information

FNIP1 variants are associated with favourable metabolism in 1 million humans

In the format provided by the authors and unedited

Supplementary Information

Table of Contents

Supplementary Notes

Supplementary Note 1. Supplementary results for the genome-wide association analysis of common variants.

Leveraging genomic data on 1,032,116 people from 11 cohorts (**Fig. 1, Supplementary Table 1, Methods**), we performed a genome-wide association study (GWAS) of TG-HDL ratio. We considered 10,753,791 common variants (minor allele frequency ≥ 1%), imputed using the TOPMed panel,[1] that passed our quality control filters (**Methods**). Using REGENIE v3.4, we fitted linear whole-genome regression models to estimate the association of each variant with TG-HDL ratio. Association estimates were generated for each cohort separately using a multi-ancestry framework and then pooled across cohorts by inverse-variance weighted fixed-effect meta-analysis (**Methods**). We also performed a sensitivity analysis where, for each cohort, we performed a GWAS separately in each ancestry and then meta-analyzed across all cohort-ancestry sets of results.

Association statistics for the meta-analysis across cohort results (main analysis), meta-analysis across cohort-ancestry results (sensitivity analysis) and for the UK Biobank (UKB) all-ancestry (ALL) analysis (main analysis of the UKB dataset) and UKB European-ancestry (EUR) only analysis (sensitivity analysis of the UKB dataset) were all consistent with appropriate control of genetic confounding (**Supplementary Table 3**), as expected for the REGENIE approach.[2] Using default EUR LD-scores and fitting the LD-score regression baseline LD model on a subset of ~1.2 million HapMap common variants, we obtained LD-score regression intercepts of 1.18, 1.19, 1.36 and 1.37 for the UKB EUR, UKB ALL, meta-analysis of cohort-ancestry results and meta-analysis of cohort results (**Supplementary Table 3**). These are similar to or lower than what was observed in analyses of similar size across multiple traits.[3] Deviations of LD-score regression intercept from 1 (up to 1.5 in UK Biobank and even higher in studies larger than UKB) are expected and have been observed in large studies in the absence of confounding and population stratification, since deviations from the theoretical model (e.g., attenuation bias) are proportional to the level of true signal and polygenicity in the study.[3] The attenuation ratio statistic, calculated as (LDSC intercept – 1) / (mean χ^2 statistic – 1), calibrates the intercept against the overall shift in χ^2 statistic due to true polygenic associations.[3] Attenuation ratio values < 0.2 have been observed in UK Biobank in optimally controlled analyses[3] and are considered reflective of adequate control for population stratification and genetic confounding.[4] We observed attenuation ratio values of ~0.11 across all the various analyses (**Supplementary Table 3**), consistent with optimal control of inflation in the context of our massive sample size and the high polygenicity of TG-HDL ratio.

We next performed fine-mapping to identify independent common variant signals associated with TG-HDL ratio. To define fine-mapping regions, we first identified variants with $P < 1\times10^{-6}$ and separated them into regions at least 100kb apart. Only regions containing at least one genome-wide significant variant ($P < 5\times10^{-8}$) were retained. Each region was then extended to the nearest recombination hotspot, with extensions ranging from 25-250kb. Finally, a 100kb buffer was applied around each region and regions with overlapping buffers were merged into a single region to form the final loci for causal variant identification. This exercise yielded 801 physical loci for fine-mapping (**Supplementary Table 4**). Next, for each locus, we computed exact linkage disequilibrium (LD) based on the exact set of individuals included in the association analysis, followed by fine-mapping using the SuSiE software (**Methods**).[5] Fine-

mapping identified 1,617 independent common sentinel variants, each of which was the variant with the highest posterior inclusion probability (PIP) for each independent credible set in each locus. Manhattan plot and QQ plots for the multi-ancestry meta-analysis are in **Supplementary Fig. 8**.

In parallel, we also performed ancestry-specific GWAS meta-analyses for five ancestry groups represented in our dataset (i.e. European, Admixed American, African, East Asian, South Asian). First we performed GWAS analyses within each cohort and ancestry group. For each ancestry, we then combined cohort-specific results into an ancestry-specific meta-analysis using inverse-variance weighted fixed-effect meta-analysis. We then performed fine-mapping separately in each ancestry using the same approach as described above and in **Methods**. This yielded 1,406 credible sets in the European analysis, 209 in the Admixed American analysis, 63 in the South Asian analysis, 44 in the African analysis and 9 in the East Asian analysis (**Supplementary Table 5 and Supplementary Figs. 9-13**).

Supplementary Note 2. Supplementary results for the exome-wide association analysis of rare coding variants.

We performed an exome-wide association analysis of TG-HDL ratio, estimating the association of rare coding variants (minor allele frequency < 1%) in each gene in the genome. In the exome-wide analysis, 60 genes were associated with TG-HDL ratio at the exome-wide level of statistical significance ($P < 1.04\times10^{-7}$; **Extended Data Table 1, Fig. 3a-b**), in an analysis adjusted for the 1,617 common variant signals identified in the same individuals (**Methods**). The exome-wide level of statistical significance was a Bonferroni correction for 20,000 genes in the genome and 24 gene-burden exposures tested for each gene (**Methods**).

We next assessed whether linkage disequilibrium between rare coding variants affected the 60 associations, noting that there were some gene-burden associations clusters (e.g. for the *APOC3*, *APOA5* and *APOA1* cluster on chromosome 11). We performed gene-burden conditional analyses adjusting the association of each of the 60 gene-burden exposures for other rare variant signals in the same chromosome (**Methods**). Of the 60 genes, 59 showed an independent association when adjusting for other gene-burden signals, whereas the association of the *AC126283.2* gene disappeared in the conditional analysis, reflecting the sequence overlap with *PLA2G12A* (**Supplementary Table 6**). The *AC126283.2* is annotated as a novel protein with no known characterization or functional details available. It is classified as a readthrough gene and tagged as a novel protein based on RNA-Seq evidence of transcription spanning the readthrough region between the *CFI* and *PLA2G12A* genes. The coding sequence (CDS) coordinates for this gene overlap with those of both *CFI* and *PLA2G12A* (Ensembl 114). Notably, *PLA2G12A* is one of the 60 genes associated with TG-HDL ratio (per-allele beta, 0.56 ratio units; 95% CI, 0.51, 0.61 ratio units; $P = 4\times10^{-109}$). In addition to the conditional analysis, accounting for *PLA2G12A- AC126283.2* sequence overlap clearly shows that *PLA2G12A* is responsible for the signal, whereas *AC126283.2* rare coding variants not shared with *PLA2G12A* have no associations with TG-HDL ratio (**Supplementary Table 8**). Therefore, *AC126283.2* cannot be considered to have an independent association with TG-HDL ratio based on our current data.

Of the 59 independent genes, 15 (25%) had been identified in the previous largest analysis of TG-HDL ratio in ~170,000 people,[6] while the remaining 44 (75%) were novel rare coding variant associations with TG-HDL ratio (**Supplementary Table 7**). In addition to the 15 overlapping genes, the previous effort[6] had reported rare coding variant associations for *APOE* and *TMEM136* (encoded by the *TLCD5* gene), which do not appear in the list of 59 independent rare variant associations from our discovery analysis (**Extended Data Table 1**). We evaluated why *APOE* and *TMEM136* (encoded by the *TLCD5* gene) were not associated in our large discovery analysis. We found that *APOE* rare variants were associated with TG-HDL ratio in our data *before* adjusting for common variants ($P = 1.1\times10^{-11}$; **Supplementary Table 9**), but this association was attenuated to below the exome-wide significance threshold *after* adjusting for common variants ($P = 0.0091$; **Supplementary Table 9**). It is important to note that the previous AJHG 2022 study did *not* adjust for common variants in their main analysis, causing the common-variant driven *APOE* signal to come through. *TMEM136* (encoded by *TLCD5*) showed no association in our exome-wide discovery analysis ($P = 0.69$; **Supplementary Table 9**), nor in the common variant unadjusted sensitivity analysis ($P = 0.80$; **Supplementary Table 9**). This is in spite of the fact that our analysis had over 3,400 rare variant carriers compared to the 157 of the AJHG 2022 paper. Therefore, it is possible that this association was a false positive in the 2022 effort.

To assess the robustness of the 59 gene-burden associations, we performed 4 sensitivity analyses using different common variant adjustment, ancestry adjustment and phenotype definition approaches. In our main analysis, gene-burden associations were adjusted for 1,617 common variant peaks identified in multi-ancestry GWAS and fine-mapping analyses. To assess the robustness of the 59 gene-burden associations to our choice of common variant adjustment approach, in the first sensitivity analysis we adjusted for common variant peaks identified in the ancestry-specific GWAS and fine-mapping instead. In this sensitivity analysis, associations were near identical as those from the main analysis (**Supplementary Table 10 and Supplementary Fig. 16a**). In the second sensitivity analysis, we did not perform any adjustment for common variants. Also here, associations were near identical as those from the main analysis (**Supplementary Table 10 and Supplementary Fig. 16b**), demonstrating robustness to the approach of common variant adjustment. In our main analysis, gene-burden associations were estimated in a multi-ancestry analysis framework. In the third sensitivity analysis, we estimated gene-burden associations in each ancestry separately and then meta-analyzed ancestry-specific association results. In this sensitivity analysis, associations were near identical as those from the main analysis (**Supplementary Table 11 and Supplementary Fig. 16c**), demonstrating the robustness of the 59 associations to the approach used to account for ancestry. In our main analysis, most TG and HDL measurements used to define the TG-HDL ratio phenotype were taken at the same time but we did allow instances where median values of TG and HDL used to define ratios were taken at different time points, which allowed for a larger discovery sample size. In the fourth sensitivity analysis, we required that measurements were taken at the same time. In this sensitivity analysis, associations were near identical as those from the main analysis (**Supplementary Table 12 and Supplementary Fig. 16d**), demonstrating robustness across different approaches to define the phenotype.

We next assessed how associations differed by ancestry for the 59 gene-burden signals. We first estimated associations separately by ancestry (**Supplementary Table 11**). We next estimated whether associations were consistent between the larger European (N = 718,681; 70.3%) vs a meta-analysis of non-European datasets (N = 302,958; 29.7%). We found that 58 of 59 genes (98%) had the same direction of association in European vs pooled non-European ancestry estimates (**Supplementary Table 11**). The only exception was the *A1CF* gene, where there was a strong association in European analyses ($P = 5.5\times10^{-27}$), but no association in the non-European subsets ($P = 0.97$), which we demonstrate is driven by a gain-of-function variant[7] that is specifically enriched in the European populations (p.Gly390Ser; **Supplementary Table 11 and Supplementary Fig. 19**). We further investigated how allelic heterogeneity and frequency differences across ancestries contributed to our signal discovery. We looked for genes where (i) *P* value in the European ancestry analysis was $> 1.04\times10^{-7}$, (ii) *P* value in any non-European ancestry analysis was <0.05 and (iii) the minor allele frequency of the gene-burden exposure was 50% larger in that same non-European ancestry compared to the European ancestry. We found three such instances (a) *PCSK9*, showing enriched frequency in African and Admixed American ancestry; (b) *LIPE*, showing enriched frequency in Admixed American ancestry; and (c) *GALNT2*, showing enriched frequency in South Asian ancestry. There were also multiple other examples using a more lenient cutoff for enriched frequency (**Supplementary Table 11**).

We assessed whether there were sex-interactions for the 59 gene-burden associations, noting that TG-HDL ratio is associated with body fat distribution, a phenotype exhibiting strong evidence of sex-interaction.[8] Association results were generally very consistent in men and women (effect size correlation

between men and women, r = 0.98, $P = 2.3\times10^{-41}$; **Supplementary Table 13 and Supplementary Fig. 17**), we detected an interesting interaction for *PDE3B*, where rare variants showed stronger association with lower TG-HDL ratio in women vs men ($I^2 = 93\%$; $P_{interaction} = 1.8\times10^{-4}$; $beta_{women}$, −0.40 vs $beta_{men}$, −0.28 SD units per allele). *PDE3B* is a known fat distribution gene showing stronger association with waist-to-hip ratio in women vs men.[9] The only other statistically significant interaction ($P < 8.5\times10^{-4}$, a Bonferroni correction for 59 genes, and $I^2 > 75\%$) was for *APOC3*, which had strong associations in both sexes in the same direction, but with different effect estimates in the context of extremely precise estimates (SD units $beta_{women}$, -0.99 vs $beta_{men}$, -1.13; $I^2 = 97\%$; $P_{interaction} = 1.0\times10^{-9}$).

As lipid levels may be affected by fasting state, we assessed whether there were interactions with fasting state for the 59 gene-burden associations and the 1,617 common fine-mapped variants. Most measures used in our discovery analysis were collected in the frame of very large epidemiological cohorts or clinical practice, where fasting state information was not collected. However, fasting state information was available in the UK Biobank subset (N = 409,602; ~40% of our discovery analysis). In UK Biobank, 104,276 samples (25%) were collected in fed state (i.e. ≤ 2 hours since last meal), 46,550 samples (11%) samples were collected in fasted state (i.e. ≥ 6 hours since last meal) and the remaining samples were collected between 2-6 hours since last meal. To estimate whether fasting state influenced our findings, we estimated associations in the fasted vs fed state subsets of UKB and tested for interaction. In this analysis, none of the 1,617 common fine-mapped variants or the 59 gene-burden signals met a Bonferroni correction for interaction ($P_{interaction} > 3.1\times10^{-5}$ for common variants and $P_{interaction} > 8.5\times10^{-4}$ for gene-burden signals), consistent with the absence of strong interactions with fasting state (**Supplementary Tables 15 and 16**).

Among the 59 genes, there was a remarkable over-representation of genes with enriched expression in liver and adipose tissues (**Fig. 3c**), which was consistent with the common variant analysis (**Supplementary Fig. 14**). The level of enrichment was far greater for the rare variant analysis compared to the common variant one, reflecting the higher confidence in causal gene identification afforded by the rare coding variant analysis.

We performed pathway enrichment analyses using DEPICT,[10] which revealed 761 enriched pathways ($P < 5.9\times10^{-6}$; **Supplementary Table 18**). There was an overwhelming representation of energy metabolism pathways including lipid and glucose homeostasis, oxygen and energy consumption, lipoprotein metabolism, insulin resistance, liver fat accumulation, lipolysis regulation, fat storage and more (**Supplementary Table 18**). For these pathways, an average of 16 (interquartile range, 11 to 19) of our 59 genes contributed to the pathway enrichment association (**Supplementary Tables 18**), reflecting an extremely high concentration of true biological signal. To dissect the contribution of different lipid fractions to TG-HDL associations and pathway enrichment, we evaluated associations with TG and HDL for the 59 genes and defined effect size balance as $|\beta_{triglycerides}| / (|\beta_{triglycerides}| + |\beta_{HDL}|)$, where genes with balance ≥ 0.75 were classified as "TG-dominant", genes with balance ≤ 0.25 classified as "HDL-dominant" and genes with balance < 0.75 and > 0.25 classified as "TG-HDL balanced" (**Methods**). As expected from our discovery approach, most genes (39 genes, 66%) were TG-HDL balanced, while 7 (12%) genes were HDL-dominant and 13 (22%) genes were TG-dominant (**Supplementary Table 19**). Genes with predominant triglyceride or HDL association showed enrichment for the respective lipoprotein particle pathways (i.e. HDL for HDL-dominant genes and VLDL and chylomicrons for triglyceride-dominant genes; **Supplementary Tables 20 and 21**), among various other pathways.

Supplementary Note 3: Mendelian disease symptom analysis for *FNIP1* and *FLCN*.

Biallelic loss-of-function variants in *FNIP1* cause *recessive* immunodeficiency-93 and hypertrophic cardiomyopathy (MIM: 619705), a syndromic immunodeficiency characterized by B-cell lymphopenia, agamma/hypogammaglobulinemia, multiple cardiac anomalies (hypertrophic cardiomyopathy, congenital cardiac disease, Wolff-Parkinson White pre-excitation syndrome), neurodevelopmental differences, muscle disease, and several other findings.[11-13]

To estimate associations between heterozygous *FNIP1* predicted loss-of-function (pLOF) variants and the features of this Mendelian syndrome, we aligned the set of clinical features reported in patients affected by *FNIP1*-related immunodeficiency syndrome[13] to our internal database of clinical phenotypes, which are derived from the structured data available in electronic health records (i.e. diagnostic/procedure codes, prescribed medications, and laboratory results). The specific *FNIP1*-related immunodeficiency syndrome features included in this study, along with their aligned EHR-derived phenotypes, are provided in **Supplementary Table 23**. We then constructed a composite phenotype of the core clinical features of the syndrome, where a core feature was any finding present in at least 20% of reported cases (**Supplementary Table 23**).[11-13] Similar to our composite cardiometabolic phenotype, individuals diagnosed with at least one of the core features were defined as cases of the composite Mendelian phenotype, whereas individuals without each of the core features were defined as controls. In the association analyses, *FNIP1* heterozygous pLOF variant carriers did not show a statistically significant association with the composite Mendelian phenotype (**Supplementary Fig. 23**). There were some nominally significant associations with individual features of the syndrome, particularly lower neutrophil counts and some electrocardiographic features (**Supplementary Fig. 24**), possibly reflecting the impact of partial *FNIP1* loss-of-function in immune and cardiac cells.

In contrast to *FNIP1,* the *FLCN* gene is associated with an autosomal *dominant* genetic disorder driven by haploinsufficiency, Birt–Hogg–Dubé syndrome (BHDS; MIM: 607273). Therefore, we hypothesized that *FLCN* heterozygous rare variant carriers in our dataset may be at higher risk for the reported clinical features of this disease.[14] To test this hypothesis, we aligned the documented clinical features of BHDS to our internal database of EHR-derived phenotypes (**Supplementary Table 24**). Also in this case, we constructed a composite phenotype of the core clinical features of BHDS, where a core feature was any finding present in at least 20% of reported cases.[14] Individuals diagnosed with at least one of the core features of BHDS were defined as cases of the composite Mendelian phenotype, whereas individuals without each of the core features were defined as controls. In the association analysis, heterozygous *FLCN* variants were associated with higher odds of the composite Mendelian phenotype (**Supplementary Fig. 23**) and were also at increased risk for several BHDS features (**Supplementary Fig. 26a**), particularly pneumothorax and renal malignancy.

In addition to the Mendelian phenotypes, we investigated associations with hepatic cancer for rare variants in *FLCN* and *FNIP1*, given the recent report of enhanced susceptibility to liver injury and carcinogenesis in mice with a hepatic knockout of *Flcn*.[15] Heterozygous variants in *FLCN* or *FNIP1* were not associated with hepatic cancer (**Supplementary Fig. 26b**).

Supplementary Figures

Supplementary Figure 1. Full scans of immunoblots on primary human hepatocytes.

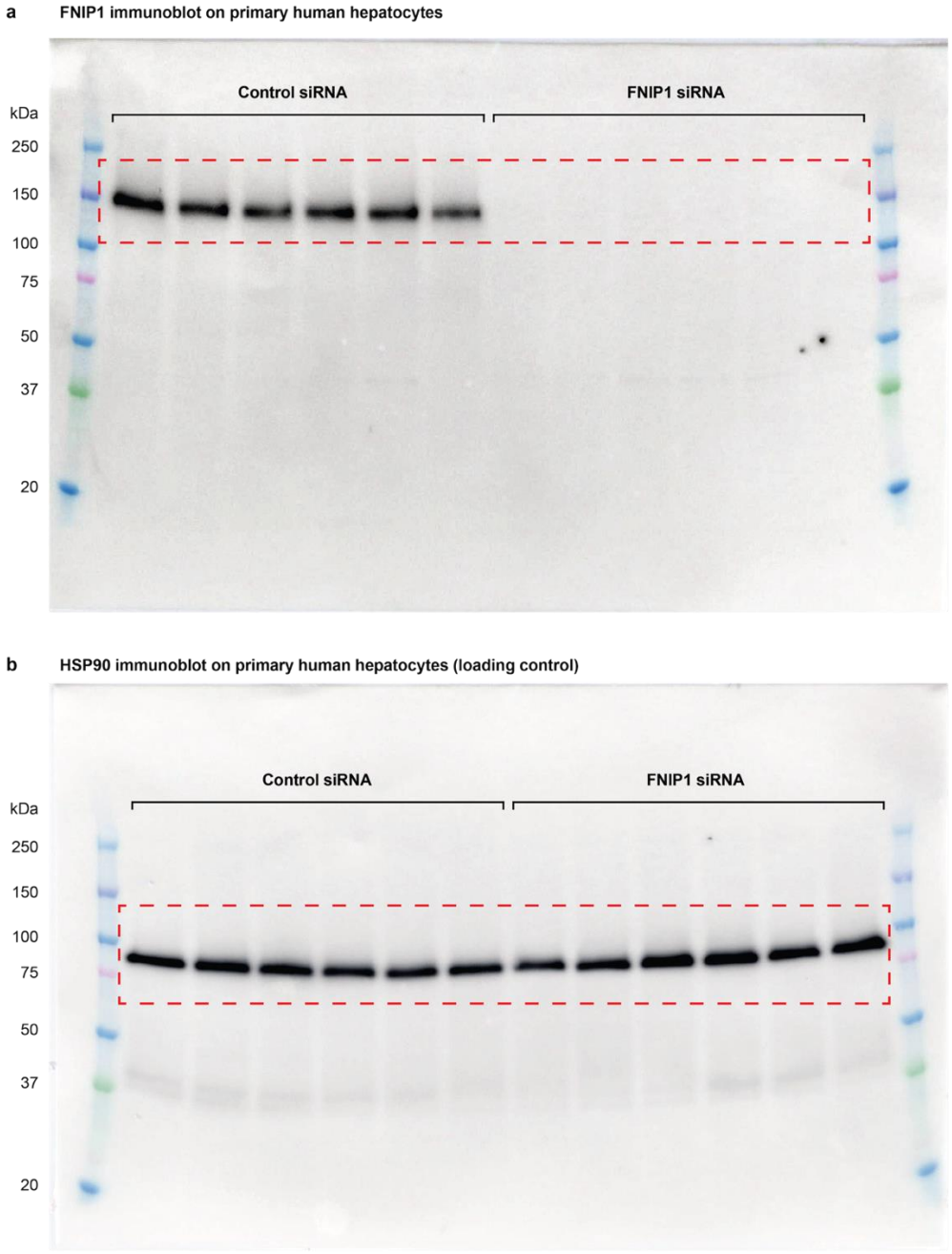

a, Immunoblot of primary human hepatocytes probed with anti-FNIP1 antibody. **b**, Immunoblot of primary human hepatocytes probed with anti-HSP90 (loading control) antibody. The loading control was run on a separate gel. Red boxes are crops included in Extended Data Fig. 5d. See also Methods.

Supplementary Figure 2. Association of TG-HDL ratio with additional anthropometric phenotypes.

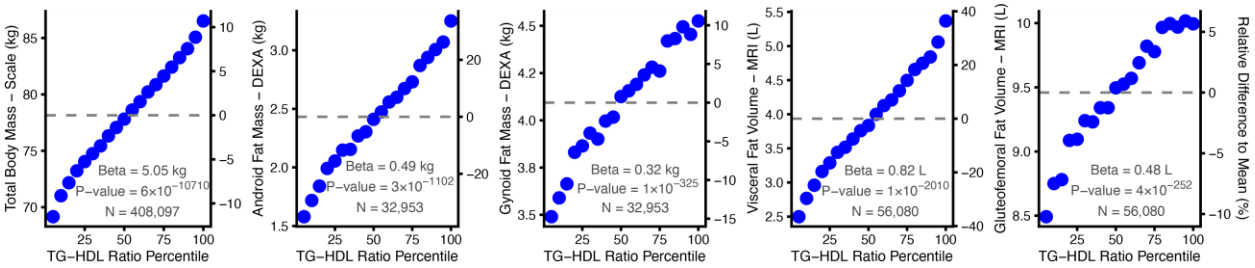

Body and fat distribution phenotypes were measured in the UKB cohort by dual-energy X-ray absorptiometry (DEXA) and magnetic resonance imaging (MRI). Associations between the TG-HDL ratio (per 1 standard deviation [SD] increase) and each outcome were estimated using linear regression adjusted for age and sex; effect estimates are shown with two-sided *P* values. No adjustment was made for multiple comparisons.

Supplementary Figure 3. Association of TG-HDL ratio with cardiometabolic phenotypes and disease risk in individuals of European ancestry.

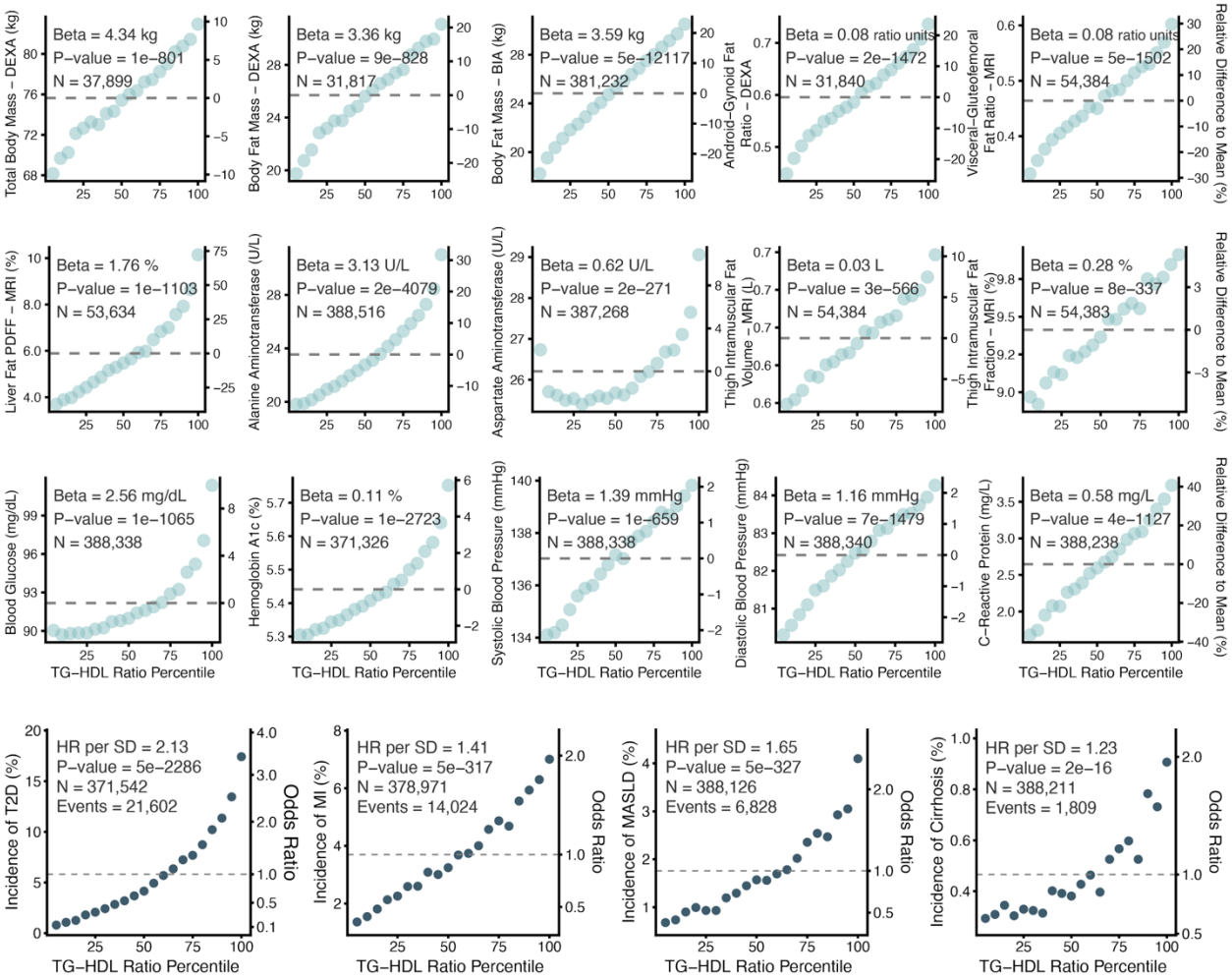

Associations were estimated in the UKB cohort. Associations between the TG-HDL ratio (per 1 standard deviation [SD] increase) and each outcome were estimated using linear regression adjusted for age and sex; effect estimates are shown with two-sided *P* values. Associations between the TG-HDL ratio (per 1 SD increase) and incident events were estimated using Cox proportional hazards models adjusted for age and sex; hazard ratios (HR) are shown with two-sided *P* values. No adjustment was made for multiple comparisons.

Supplementary Figure 4. Association of TG-HDL ratio with cardiometabolic phenotypes and disease risk in individuals of South Asian ancestry.

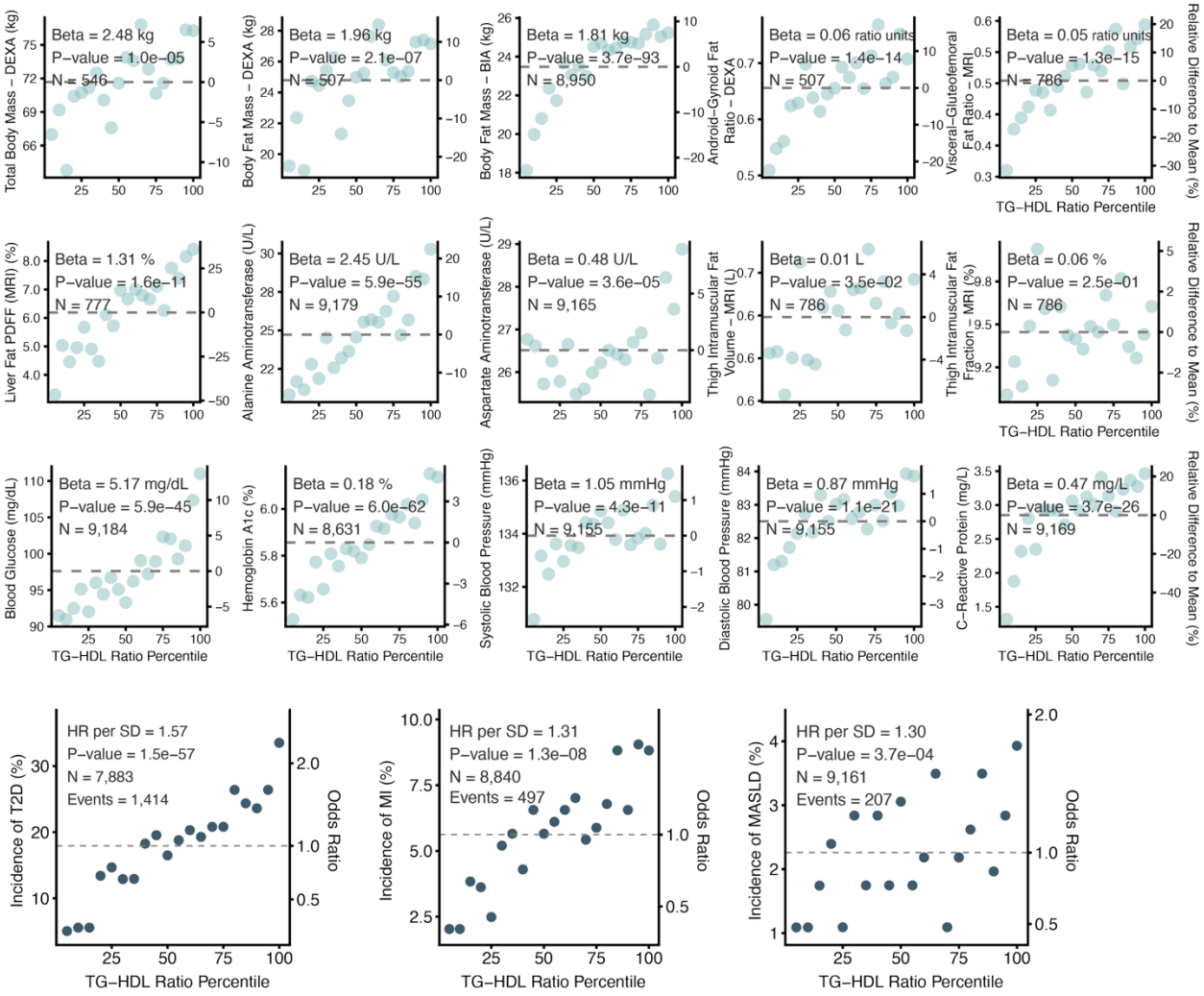

Associations were estimated in the UKB cohort. To allow sufficient statistical power to estimate associations, phenotypes available in less than 500 individuals or binary outcome phenotypes with less than 100 incident cases in South Asian ancestry participants were not analyzed. Associations between the TG-HDL ratio (per 1 standard deviation [SD] increase) and each outcome were estimated using linear regression adjusted for age and sex; effect estimates are shown with two-sided *P* values. Associations between the TG-HDL ratio (per 1 SD increase) and incident events were estimated using Cox proportional hazards models adjusted for age and sex; hazard ratios (HR) are shown with two-sided *P* values. No adjustment was made for multiple comparisons.

Supplementary Figure 5. Association of TG-HDL ratio with cardiometabolic phenotypes and disease risk in individuals of African ancestry.

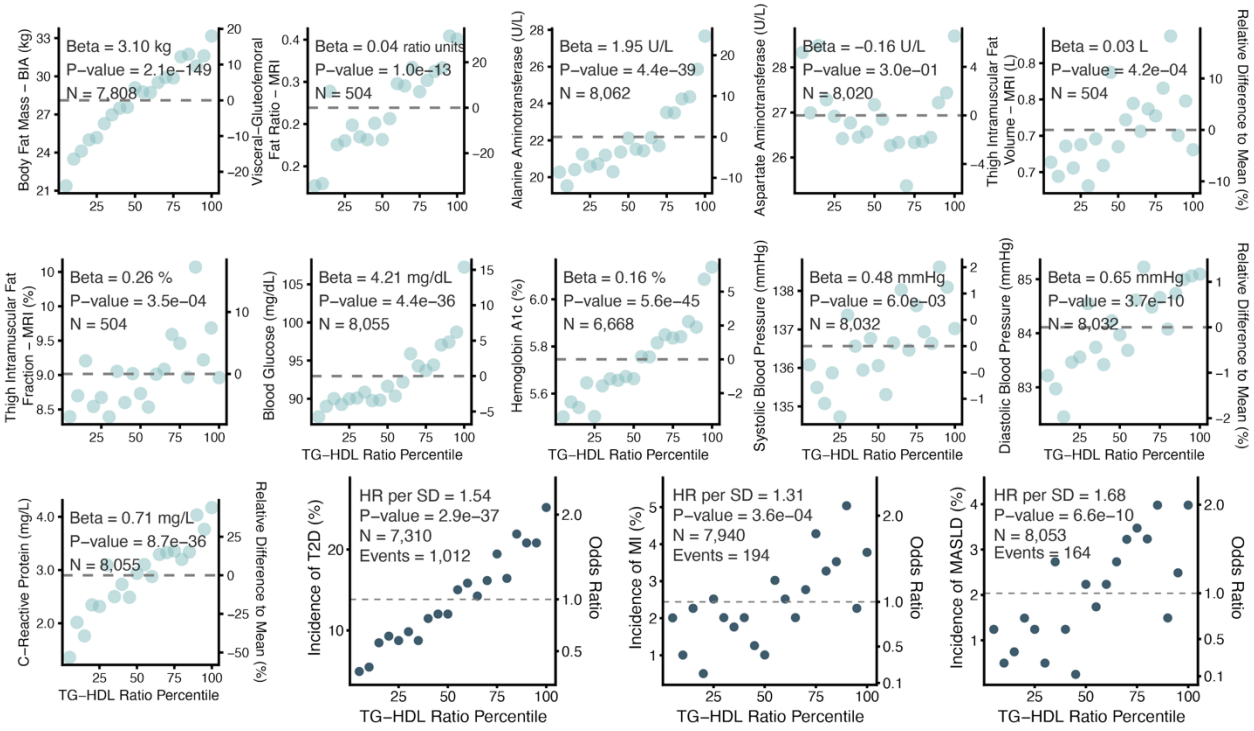

Associations were estimated in the UKB cohort. To allow sufficient statistical power to estimate associations, phenotypes available in less than 500 individuals or binary outcome phenotypes with less than 100 incident cases in African ancestry participants were not analyzed. Associations between the TG-HDL ratio (per 1 standard deviation [SD] increase) and each outcome were estimated using linear regression adjusted for age and sex; effect estimates are shown with two-sided *P* values. Associations between the TG-HDL ratio (per 1 SD increase) and incident events were estimated using Cox proportional hazards models adjusted for age and sex; hazard ratios (HR) are shown with two-sided *P* values. No adjustment was made for multiple comparisons.

Supplementary Figure 6. Association of TG-HDL ratio with cardiometabolic phenotypes and disease risk in individuals of East Asian ancestry.

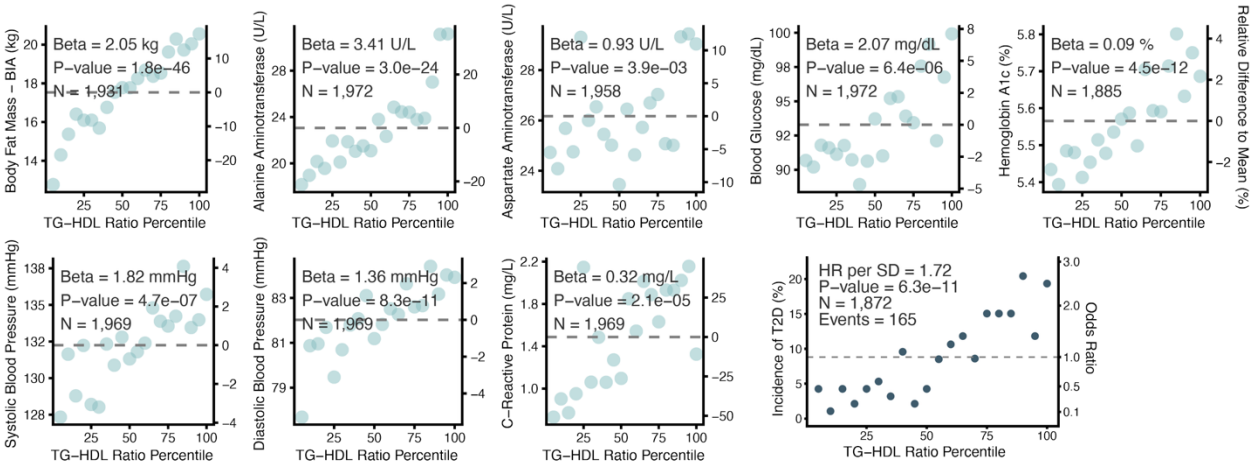

Associations were estimated in the UKB cohort. To allow sufficient statistical power to estimate associations, phenotypes available in less than 500 individuals or binary outcome phenotypes with less than 100 incident cases in East Asian ancestry participants were not analyzed. Associations between the TG-HDL ratio (per 1 standard deviation [SD] increase) and each outcome were estimated using linear regression adjusted for age and sex; effect estimates are shown with two-sided *P* values. Associations between the TG-HDL ratio (per 1 SD increase) and incident events were estimated using Cox proportional hazards models adjusted for age and sex; hazard ratios are (HR) shown with two-sided *P* values. No adjustment was made for multiple comparisons.

Supplementary Figure 7. Association of TG-HDL ratio with cardiometabolic phenotypes and disease risk in individuals of Admixed American ancestry.

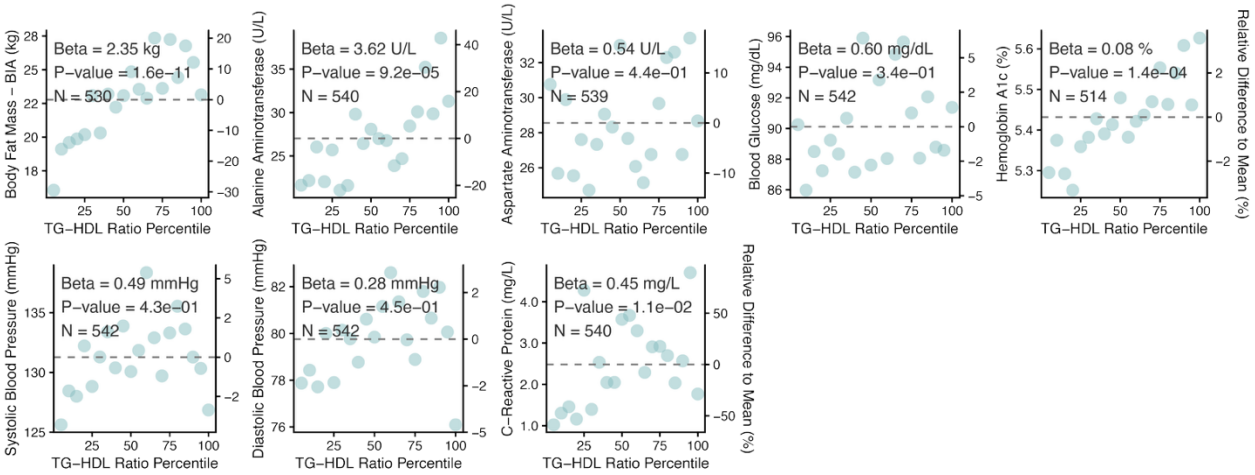

Associations were estimated in the UKB cohort. To allow sufficient statistical power to estimate associations, phenotypes available in less than 500 individuals or binary outcome phenotypes with less than 100 incident cases in Admixed American ancestry participants were not analyzed. Associations between the TG-HDL ratio (per 1 standard deviation [SD] increase) and each outcome were estimated using linear regression adjusted for age and sex; effect estimates are shown with two-sided *P* values. No adjustment was made for multiple comparisons.

Supplementary Figure 8. Association of common variants with TG-HDL ratio in the all-ancestry meta-analysis.

Panel a.

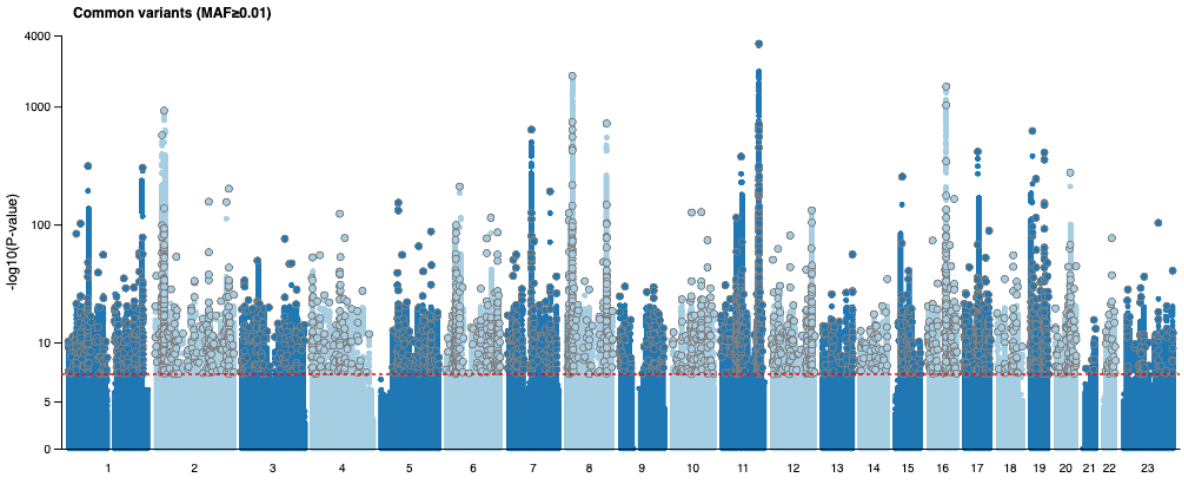

Panel b.

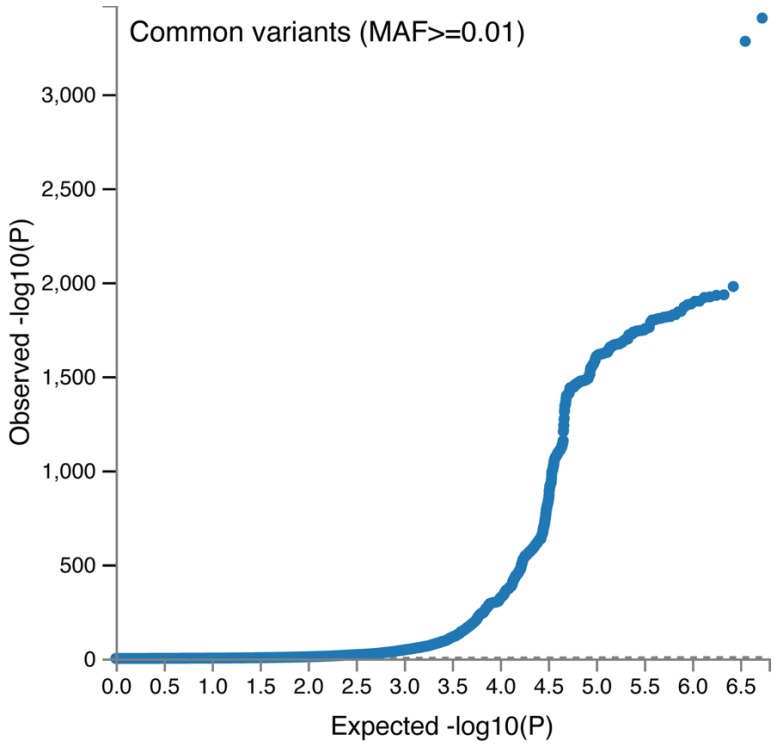

a, Manhattan plot. **b,** QQ plot. Associations are from inverse-variance weighted fixed-effect meta-analysis and *P* values are from two-sided Wald tests for variants with minor allele frequency (MAF) higher than 1%.

Supplementary Figure 9. Association of common variants with TG-HDL ratio in the European ancestry meta-analysis.

Panel a.

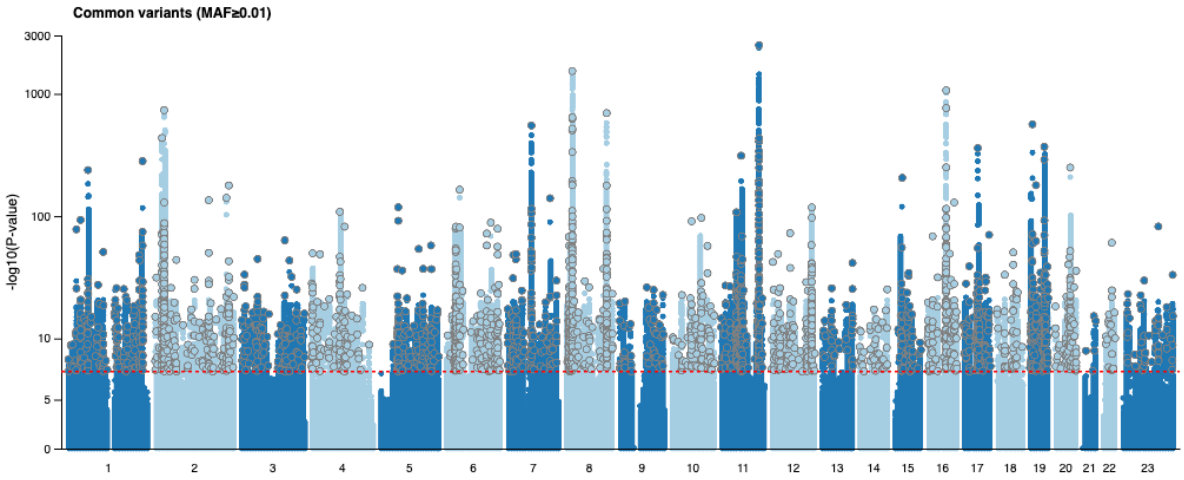

Panel b.

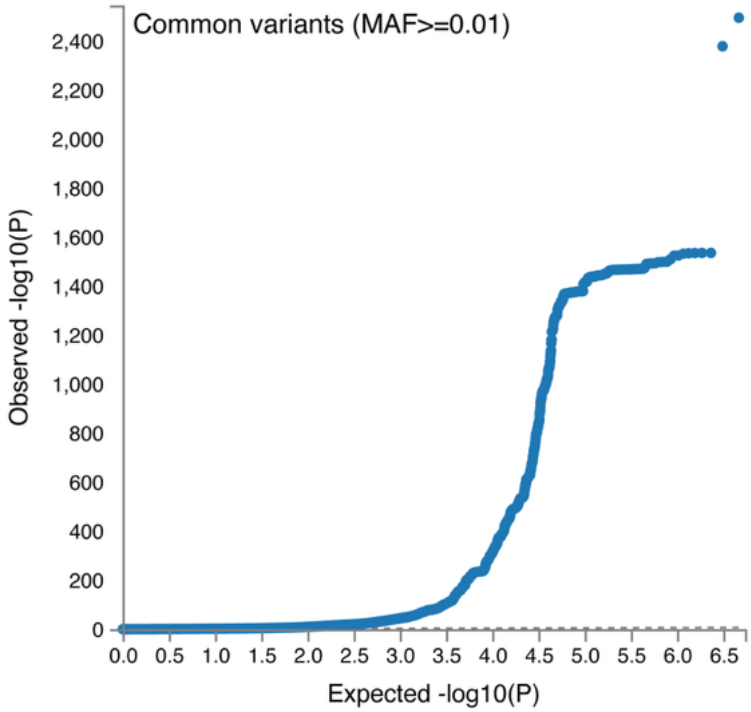

a, Manhattan plot. **b,** QQ plot. Associations are from inverse-variance weighted fixed-effect meta-analysis and *P* values are from two-sided Wald tests for variants with minor allele frequency (MAF) higher than 1%.

Supplementary Figure 10. Association of common variants with TG-HDL ratio in the Admixed American ancestry meta-analysis.

Panel a.

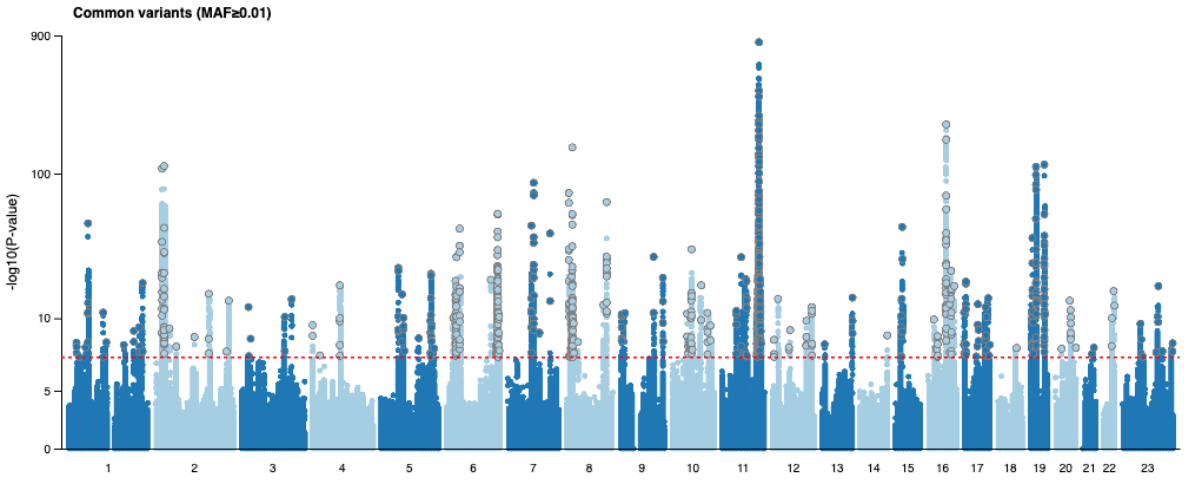

Panel b.

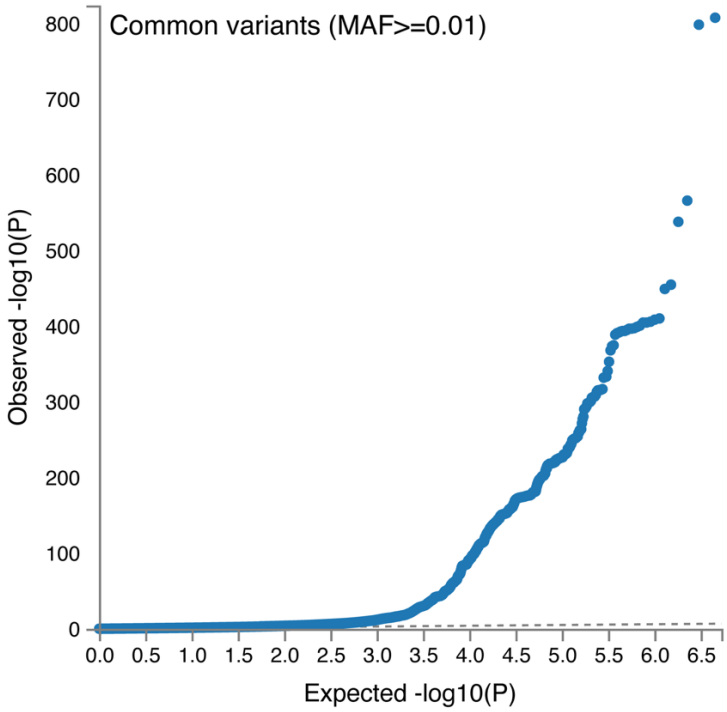

a, Manhattan plot. **b,** QQ plot. Associations are from inverse-variance weighted fixed-effect meta-analysis and *P* values are from two-sided Wald tests for variants with minor allele frequency (MAF) higher than 1%.

Supplementary Figure 11. Association of common variants with TG-HDL ratio in the South Asian ancestry meta-analysis.

Panel a.

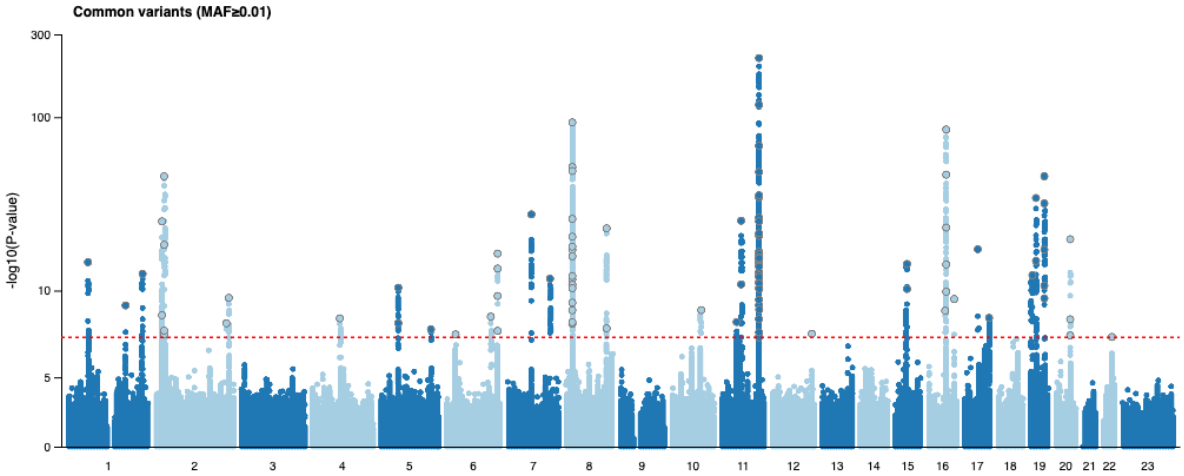

Panel b.

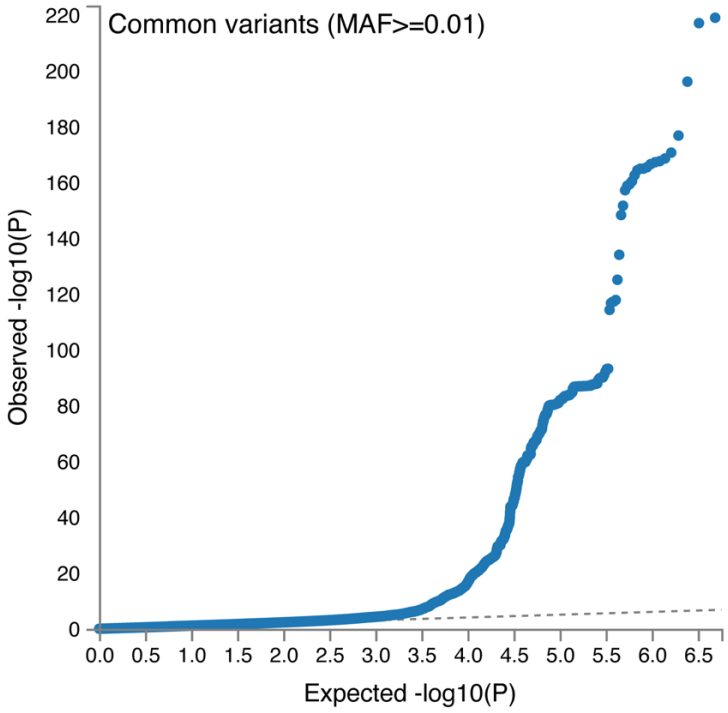

a, Manhattan plot. **b,** QQ plot. Associations are from inverse-variance weighted fixed-effect meta-analysis and *P* values are from two-sided Wald tests for variants with minor allele frequency (MAF) higher than 1%.

Supplementary Figure 12. Association of common variants with TG-HDL ratio in the African ancestry meta-analysis.

Panel a.

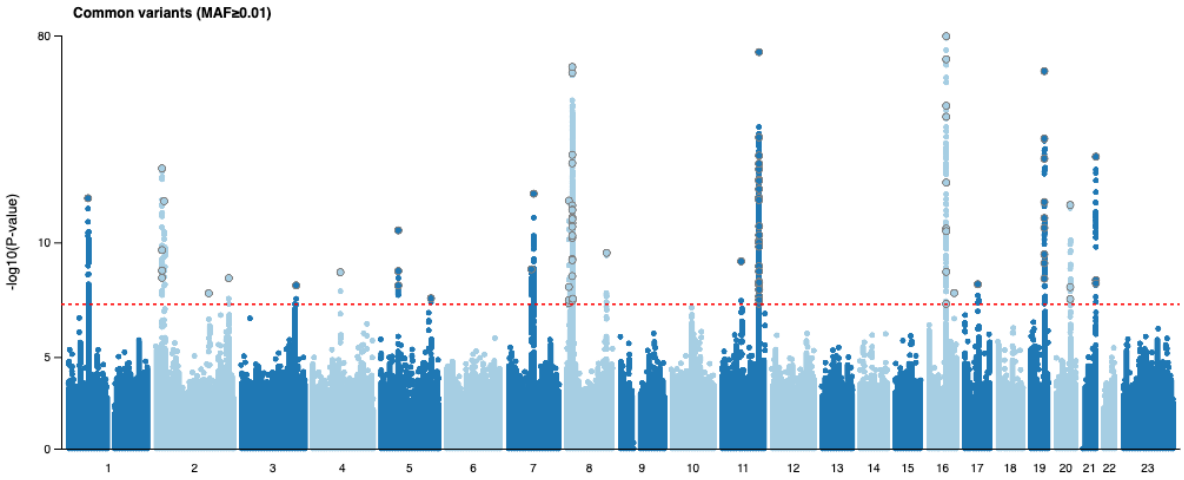

Panel b.

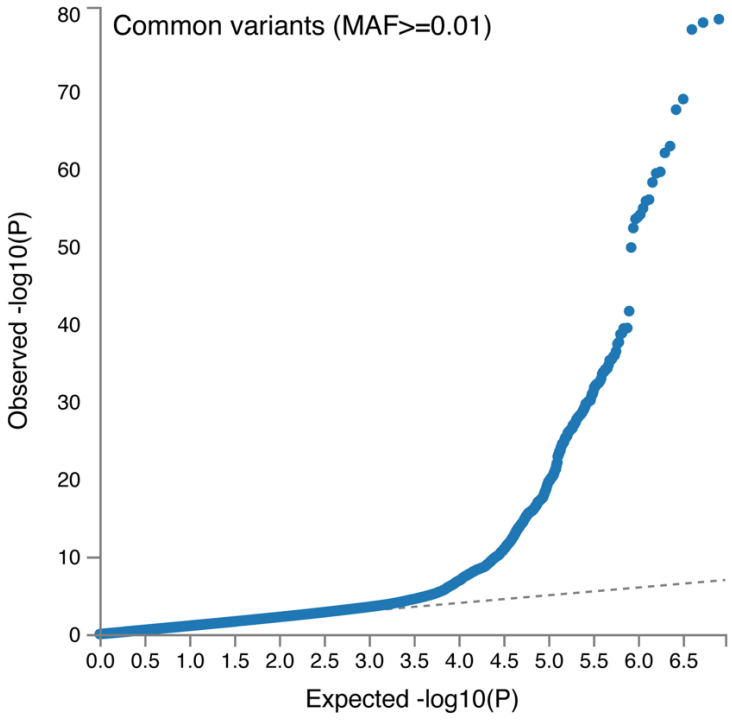

a, Manhattan plot. **b,** QQ plot. Associations are from inverse-variance weighted fixed-effect meta-analysis and *P* values are from two-sided Wald tests for variants with minor allele frequency (MAF) higher than 1%.

Supplementary Figure 13. Association of common variants with TG-HDL ratio in the East Asian ancestry meta-analysis.

Panel a.

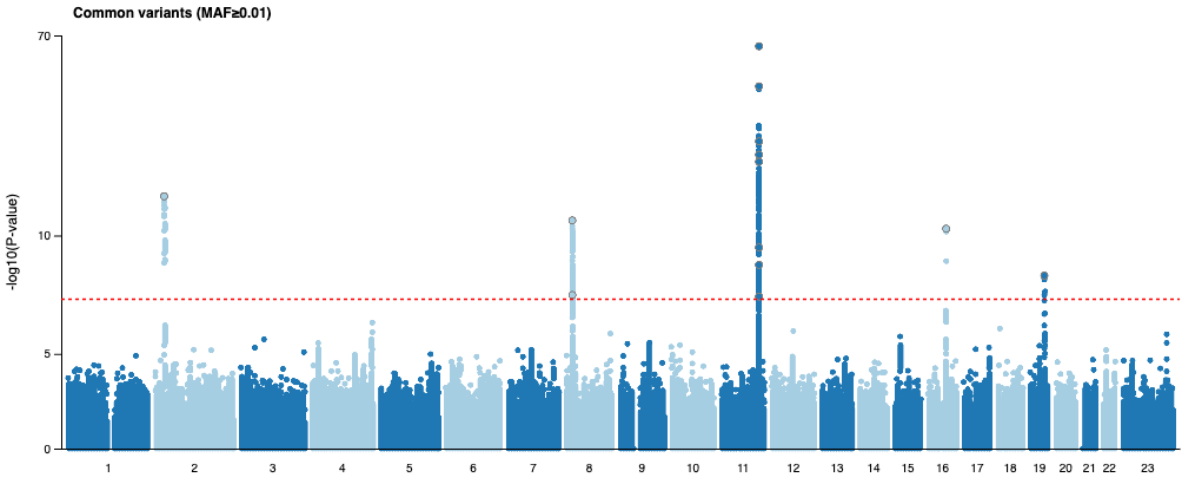

Panel b.

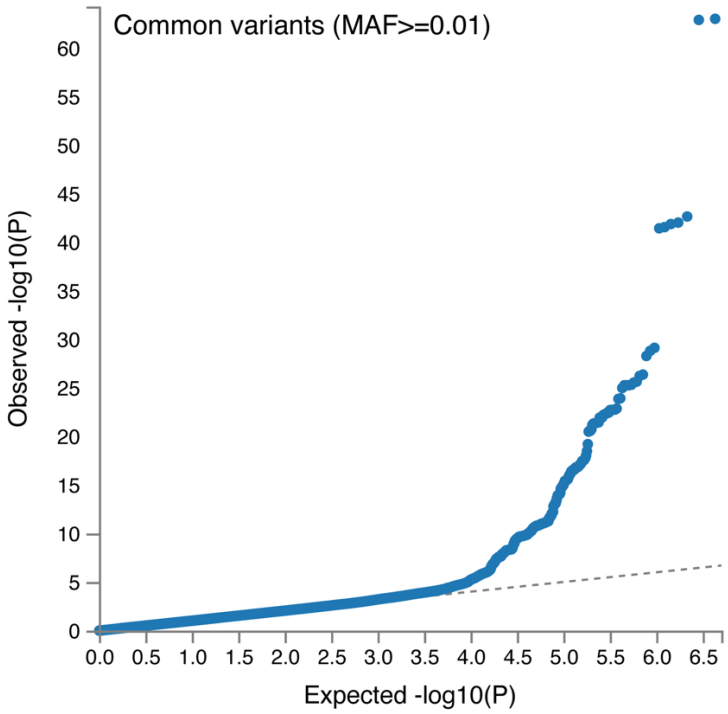

a, Manhattan plot. **b,** QQ plot. Associations are from inverse-variance weighted fixed-effect meta-analysis and *P* values are from two-sided Wald tests for variants with minor allele frequency (MAF) higher than 1%.

Supplementary Figure 14. Tissue enrichment analysis for the common variant genome-wide analysis of TG-HDL ratio.

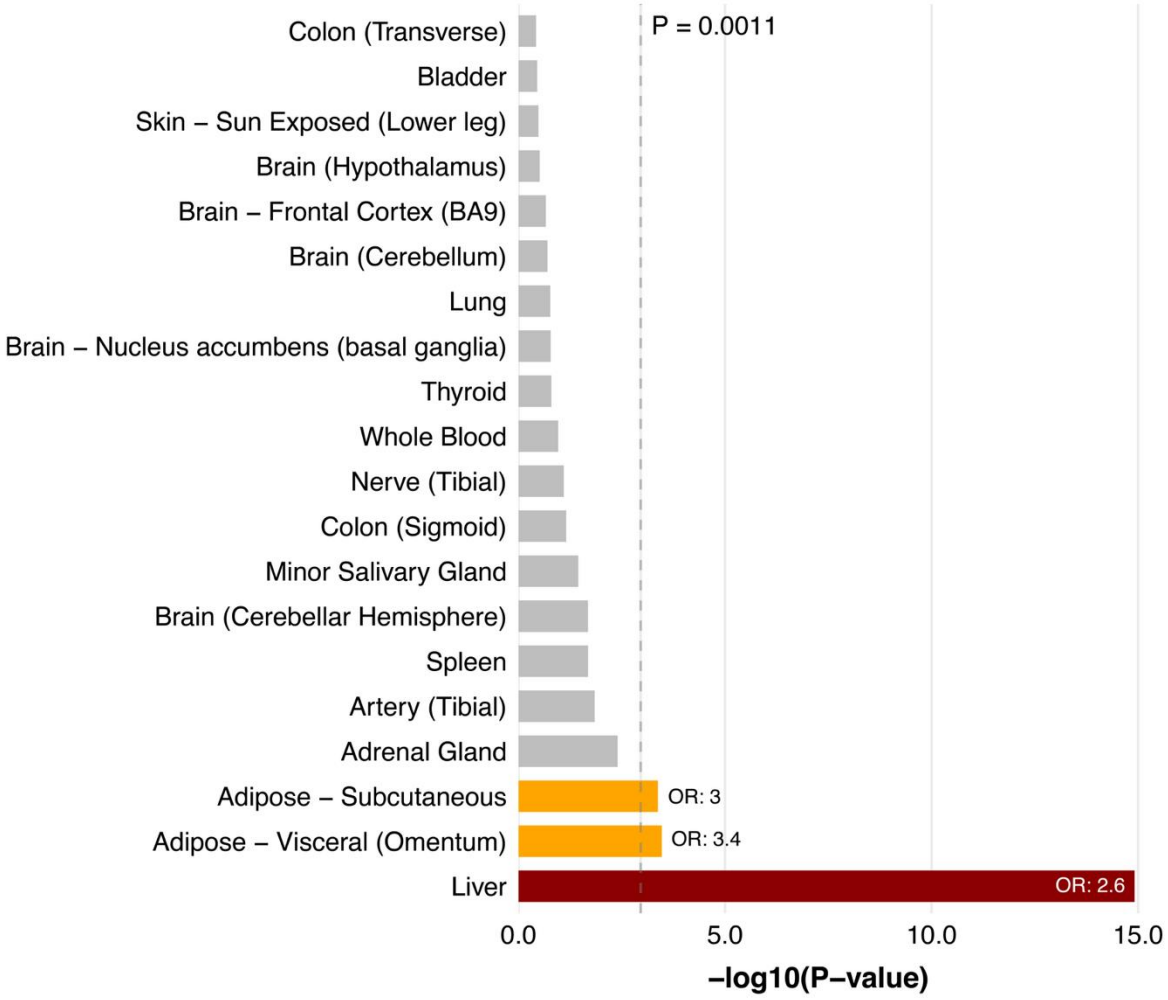

Each tissue-specific enrichment odds ratio (OR) represents the likelihood of being a GWAS-prioritized gene exhibiting expression enrichment in a given tissue, relative to genes lacking such enrichment in that tissue (see Methods for full details). The plot shows the top 20 tissues. The enrichment ORs and *P* values were obtained a one-sided penalized likelihood ratio test from the Firth-corrected logistic model.

Supplementary Figure 15. Association with cardiometabolic phenotypes of a polygenic risk score for TG-HDL ratio, built with common fine-mapped variants identified in our study.

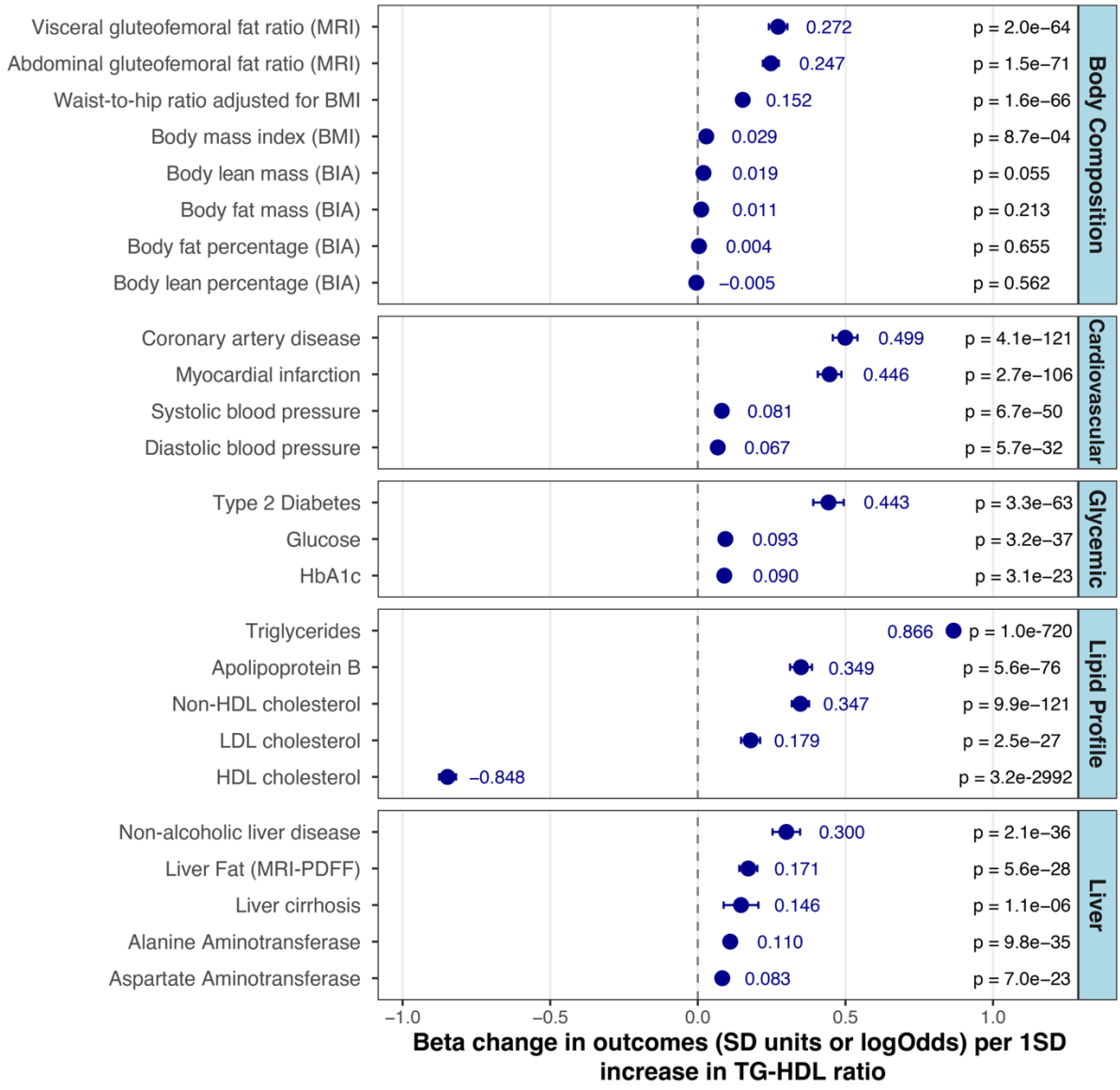

Associations (Beta ± 95% CI) and two-sided *P* values were obtained from inverse-variance weighted Mendelian randomization analysis using estimates from 1,617 finemapped TG-HDL ratio variants on TG-HDL in standard deviation (SD) units as exposure and on several cardiometabolic outcomes in SD units for quantitative traits and logOdds units for binary traits. BIA, bioimpedance; BMI, body mass index; Hba1c, hemoglobin A1c; MRI, magnetic resonance imaging; PDFF, proton density fat fraction.

Supplementary Figure 16. Robustness of main analysis associations after sensitivity analyses.

Panel a.

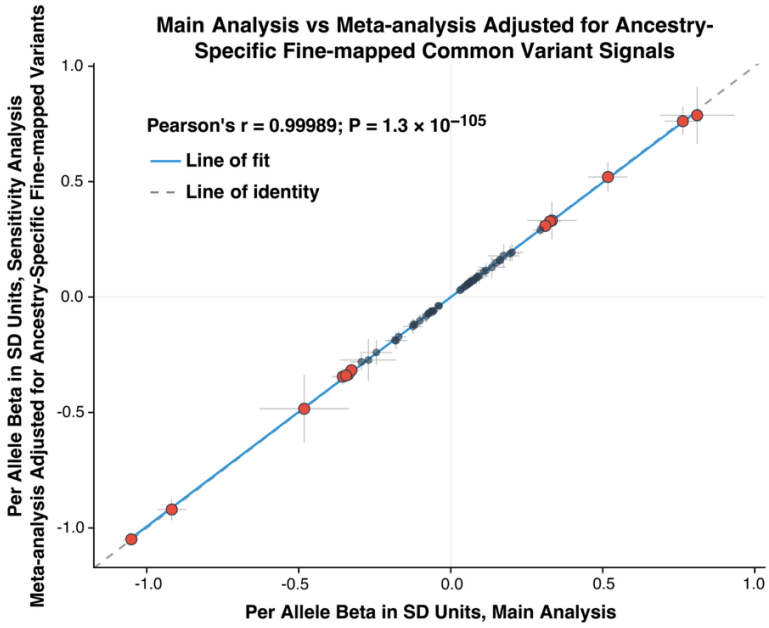

Panel b.

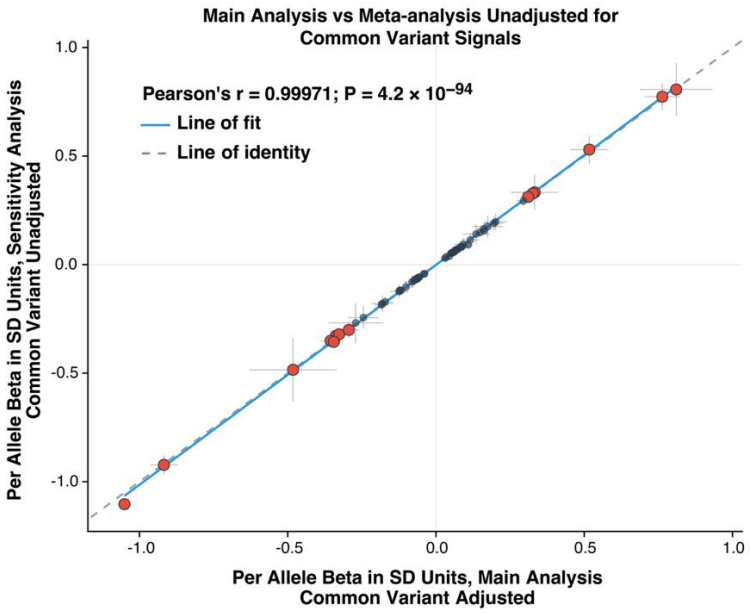

Panel c.

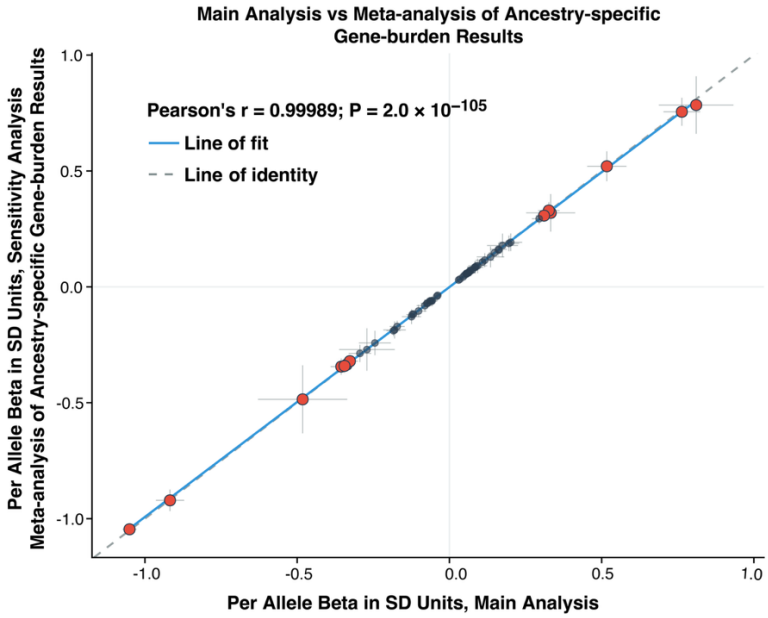

Panel d.

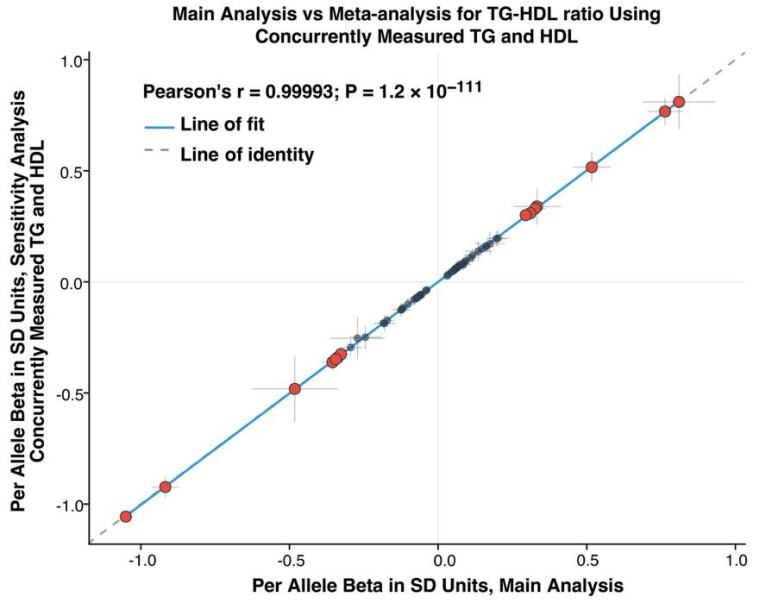

Concordance of per-allele effect estimates for the top 59 rare variant gene masks between main meta-analysis and **a**, meta-analysis of ancestry-specific results adjusted for common ancestry-specific fine-mapped variants, **b**, meta-analysis unadjusted for common variants, **c**, meta-analysis of ancestry-specific results adjusted for 1,617 common fine-mapped variants from multi-ancestry meta-analysis, and **d**, meta-analysis of TG-HDL ratio with TG and HDL measured from same blood draw. Pearson's correlation coefficients and two-sided *P* values are shown for each comparison.

Supplementary Figure 17. Concordance of TG-HDL ratio associations between men and women.

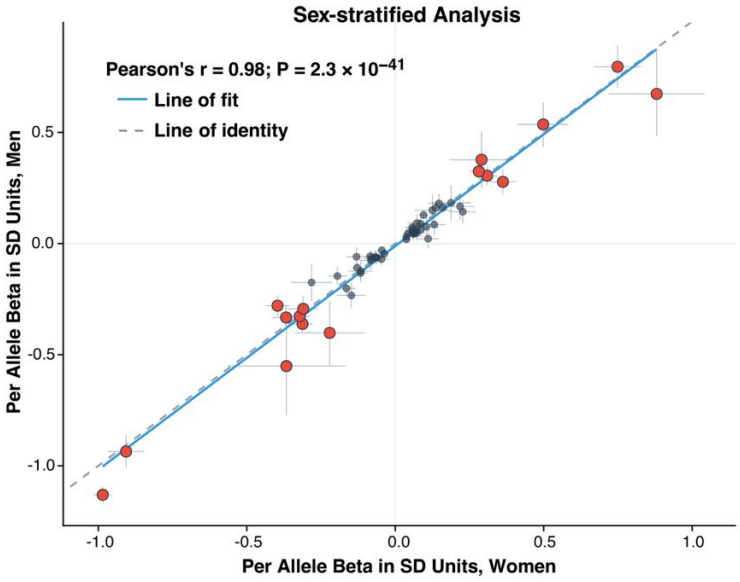

Concordance of per-allele effect estimates for the top 59 rare variant gene masks between sex-stratified meta-analyses in men versus women. Pearson's correlation coefficient and two-sided *P* value are shown.

Supplementary Figure 18. Replication of TG-HDL ratio associations in the All of Us cohort.

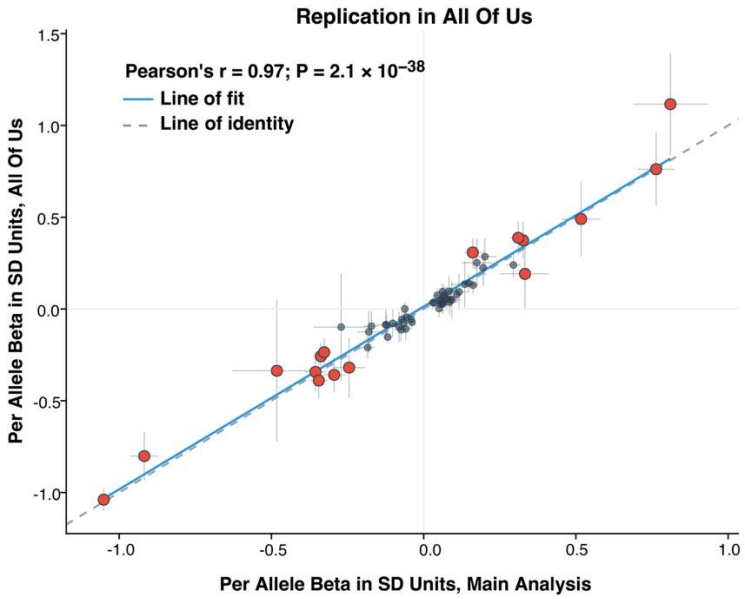

Concordance of effects for the top 59 rare variant gene masks between main meta-analysis and analysis with TG-HDL ratio in the All of Us cohort. Pearson's correlation coefficient and two-sided *P* value are shown.

Supplementary Figure 19. Association of *A1CF* rare loss-of-function plus deleterious missense variants with TG-HDL ratio by ancestry reveals that overall signal is driven by p.Gly390Ser variant.

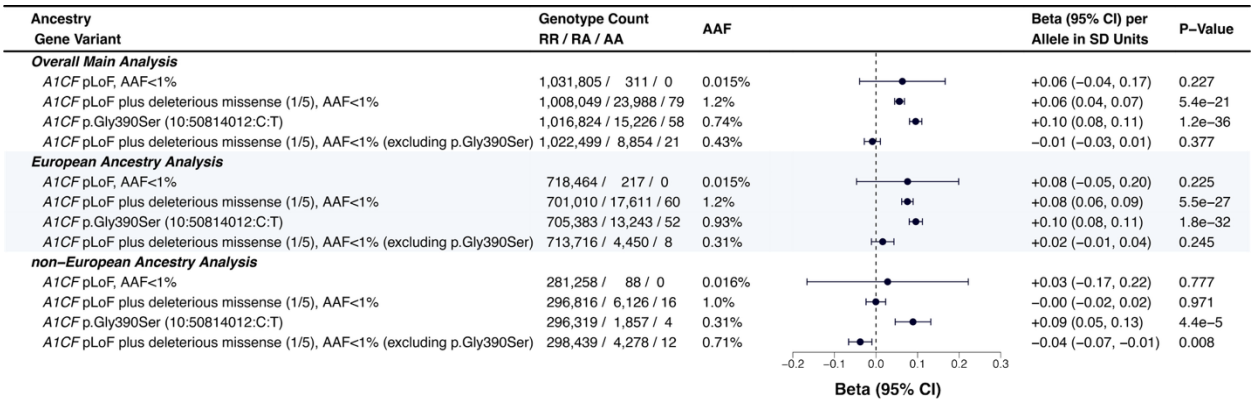

Associations are shown in per-allele change in standard deviation (SD) units (Beta ± 95% CI). Association estimates are from inverse-variance weighted fixed-effect meta-analysis and *P* values are from two-sided Wald tests. AAF, alternative allele frequency; CI, confidence interval; pLOF, predicted loss-of-function; RR, homozygous for the reference allele; RA, heterozygous; AA, homozygous for the alternative allele.

Supplementary Figure 20. Association of predicted loss-of-function variants in 13 genes with the respective protein levels.

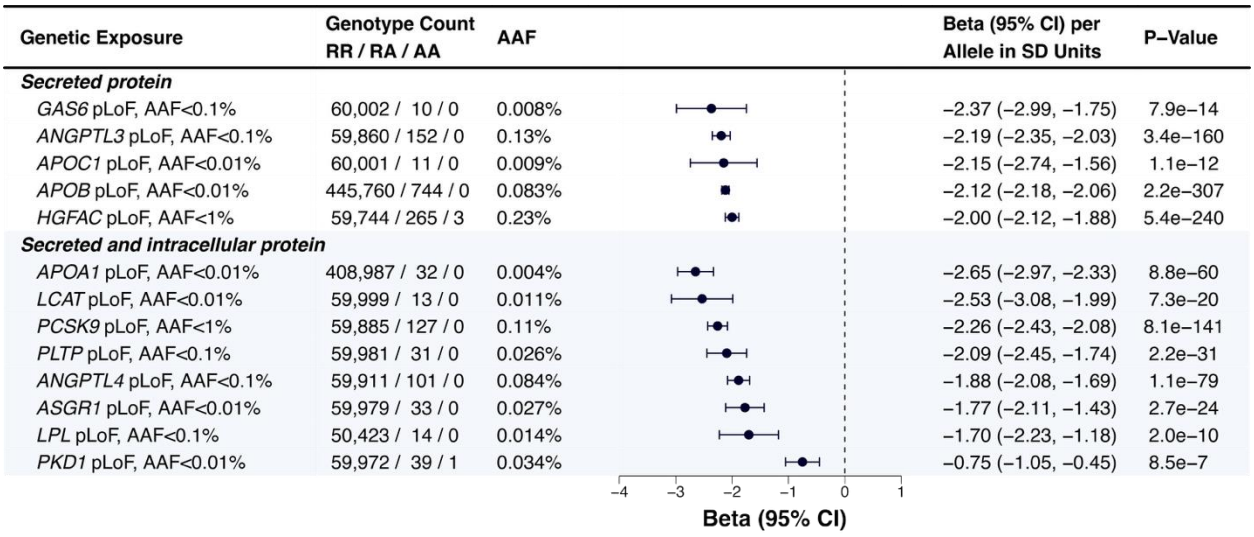

Out of the 59 proteins encoded by top TG-HDL ratio genes, 13 were annotated as "secreted" in Human Protein Atlas and were measured by Olink proteomics in UK Biobank and the Geisinger Health System or by immunoassay (for APOB and APOA1) in the UK Biobank. Associations are shown in per allele change in standard deviation (SD) units (Beta ± 95% CI). Association estimates are from inverse-variance weighted fixed-effect meta-analysis and *P* values are from two-sided Wald tests. AAF, alternative allele frequency; CI, confidence interval; pLOF, predicted loss-of-function; RR, homozygous for the reference allele; RA, heterozygous; AA, homozygous for the alternative allele.

Supplementary Figure 21. Association of 59 TG-HDL ratio genes with cardiometabolic traits.

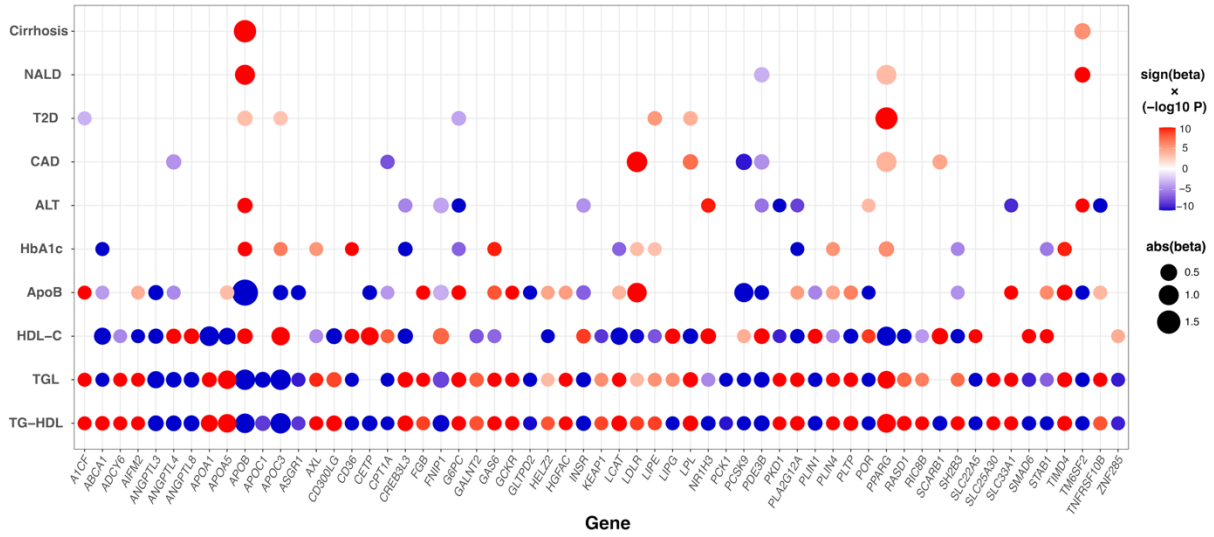

Direction of effect is shown on a spectrum where positive associations are shown in red and negative associations are shown in blue and the size of each point is proportional to the effect size obtained from beta in standard deviation units for quantitative traits and the ln(odds ratio) for binary traits. Associations are shown for estimates with *P* values < 0.001 for the best rare variant gene-burden (as listed in Table 1 for each gene). Association estimates are from inverse-variance weighted fixed-effect meta-analysis and *P* values are from the gene-burden test with the lowest two-sided Wald test *P* value per gene. ALT, alanine aminotransferase; ApoB, apolipoprotein B; CAD, coronary artery disease; HbA1c, hemoglobin A1c; HDL-C, high-density lipoprotein cholesterol; MASLD; metabolic dysfunction-associated steatotic liver disease; T2D, type 2 diabetes, TG-HDL, triglycerides to HDL cholesterol ratio; TGL, triglycerides.

Supplementary Figure 22. Rare predicted loss-of-function variants contributing to the *FNIP1* gene-burden association with TG-HDL ratio.

Panel a.

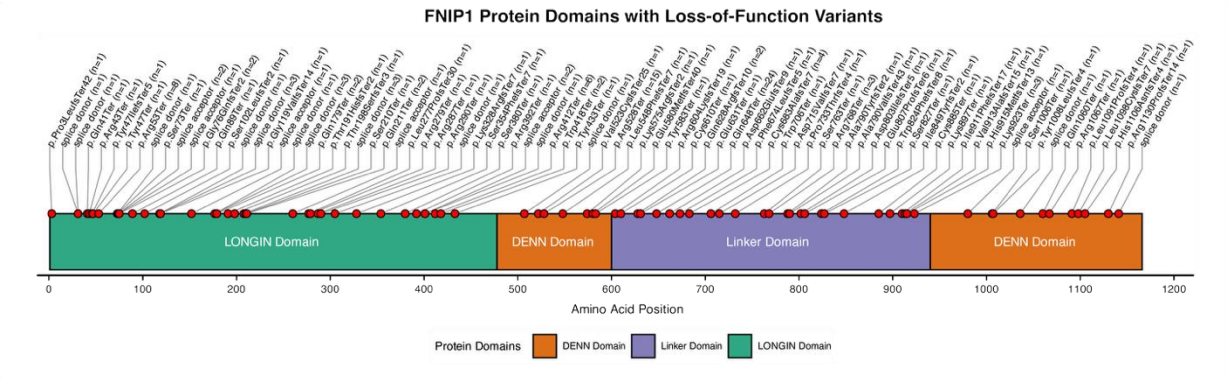

Panel b.

FNIP1 pLoF, AAF<0.01%

Gene Variant	Genotype Count RR / RA / AA	AAF	Beta (95% CI) per Allele in Clinical Units	P–Value	Heterogeneity P-Value
All Variants	1,031,961 / 155 / 0	0.008%	−1.66 (−2.17, −1.16) ratio	1.1e−10	
NMD classification					
NMD Variants	1,031,511 / 126 / 0	0.006%	−1.62 (−2.18, −1.06) ratio	1.5e−8	0.81
Non−NMD/splice site Variants	931,010 / 29 / 0	0.002%	−1.88 (−3.05, −0.71) ratio	0.002	
Location of pLOF mutation					
N−Terminus Variants	1,026,423 / 68 / 0	0.003%	−1.96 (−2.72, −1.20) ratio	4.4e−7	0.32
C−Terminus Variants	1,031,549 / 87 / 0	0.004%	−1.43 (−2.11, −0.76) ratio	3.1e−5	

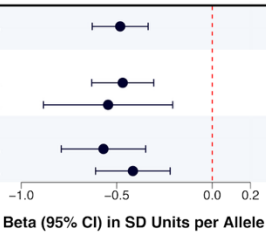

a, Predicted loss-of-function (pLOF) variants in *FNIP1* identified by exome sequencing mapped to the respective protein domains. **b**, Gene-burden analyses for subgroups of pLOF variants annotated according to variant position (N- versus C- terminus) or predicted non-sense mediated decay (NMD) status. We estimated heterogeneity in genetic associations between variant groups, showing that *FNIP1* pLOF variants with different annotations (N- vs C-terminus or NMD vs non-NMD) were robustly and consistently associated with lower TG-HDL ratio ($P_{\text{heterogeneity}} > 0.32$ for each comparison). Variants located at or before the transcript midpoint (amino acid position ≤583) were classified as N-terminal variants; the remainder were classified as C-terminal variants. Association estimates are from inverse-variance weighted fixed-effect meta-analysis and *P* values are from two-sided Wald tests. Heterogeneity *P* values are based on Cochran's Q statistic, evaluated with a chi-squared distribution with 11 degrees of freedom. See Methods for NMD variant definition. AAF, alternative allele frequency; CI, confidence interval; NMD, non-sense mediated decay; pLOF, predicted loss-of-function; RR, homozygous for the reference allele; RA, heterozygous; AA, homozygous for the alternative allele.

Supplementary Figure 23. Association of *FNIP1* and *FLCN* variants with cardiometabolic and Mendelian composite phenotypes.

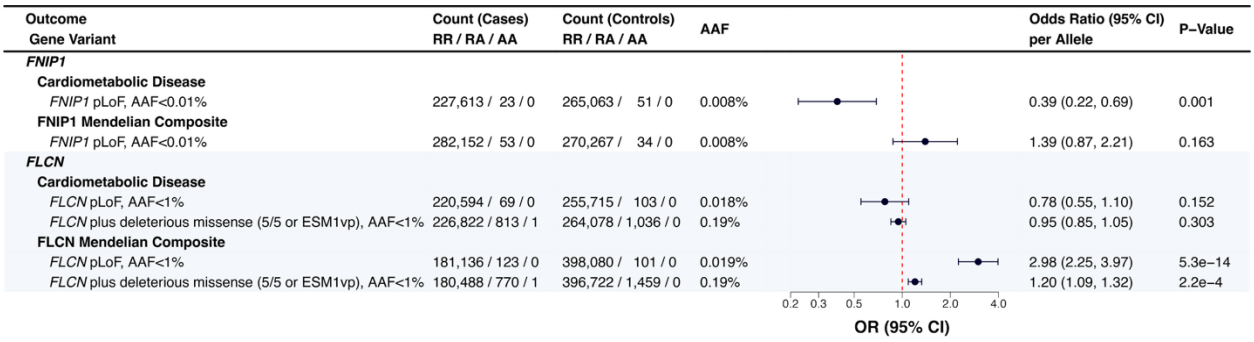

For the composite cardiometabolic phenotype, case status was defined as being a case of coronary artery disease, type 2 diabetes or liver disease (i.e. MASLD or liver cirrhosis), while control status was defined as being a control for each of those diseases. The FNIP1 Mendelian composite phenotype was a combination of the key clinical features of immunodeficiency-93 and hypertrophic cardiomyopathy (see Supplementary Note 3 and Supplementary Table 23), whereas the FLCN Mendelian composite phenotype was a combination of the key clinical features of Birt–Hogg–Dubé syndrome (see Supplementary Note 3 and Supplementary Table 24). Association estimates are from inverse-variance weighted fixed-effect meta-analysis and *P* values are from two-sided Wald tests. AAF, alternative allele frequency; CI, confidence interval; OR, odds ratio; pLOF, predicted loss-of-function; RR, homozygous for the reference allele; RA, heterozygous; AA, homozygous for the alternative allele.

Supplementary Figure 24. Association of heterozygous pLOF variants in *FNIP1* with individual phenotypes described in autosomal recessive FNIP1-related immunodeficiency syndrome.

Panel a.

Outcome Gene Variant	Count (Cases) RR / RA / AA	Count (Controls) RR / RA / AA	AAF	Odds Ratio (95% CI) per Allele	P–Value
CNS: Congenital Malformations of Brain					
FNIP1 pLoF, AAF<0.01%	1,634 / 0 / 0	499,511 / 72 / 0	0.007%	0.4 (0.0, 26.7)	0.642
CNS: Developmental Delay					
FNIP1 pLoF, AAF<0.01%	10,814 / 2 / 0	974,209 / 144 / 0	0.007%	2.1 (0.5, 8.6)	0.295
CNS: Microcephaly					
FNIP1 pLoF, AAF<0.01%	183 / 0 / 0	168,892 / 20 / 0	0.006%	–	0.955
Cardiac: Congenital Heart Disease					
FNIP1 pLoF, AAF<0.01%	3,834 / 1 / 0	1,012,148 / 147 / 0	0.007%	3.8 (0.6, 23.1)	0.146
Cardiac: Hypertrophic Cardiomyopathy					
FNIP1 pLoF, AAF<0.01%	3,420 / 1 / 0	592,698 / 88 / 0	0.007%	3.4 (0.5, 20.9)	0.189
Cardiac: Pre–excitation Syndrome					
FNIP1 pLoF, AAF<0.01%	1,418 / 0 / 0	902,875 / 127 / 0	0.007%	0.4 (0.0, 74.0)	0.711
Cardiac: Wolff–Parkinson–White Syndrome					
FNIP1 pLoF, AAF<0.01%	1,319 / 0 / 0	744,005 / 94 / 0	0.006%	0.4 (0.0, 38.0)	0.671
Gastrointestinal: Crohn's Disease					
FNIP1 pLoF, AAF<0.01%	9,397 / 1 / 0	961,381 / 141 / 0	0.007%	1.7 (0.4, 8.1)	0.496
Gastrointestinal: Inflammatory Bowel Disease					
FNIP1 pLoF, AAF<0.01%	19,940 / 2 / 0	961,381 / 141 / 0	0.007%	1.0 (0.3, 3.0)	0.982
Hematologic: Anemias					
FNIP1 pLoF, AAF<0.01%	189,711 / 31 / 0	875,325 / 128 / 0	0.007%	1.0 (0.7, 1.5)	0.979
Immune: Common Bacterial Infections					
FNIP1 pLoF, AAF<0.01%	26,328 / 6 / 0	1,034,406 / 153 / 0	0.007%	1.9 (0.8, 4.5)	0.136
Immune: Neutropenia					
FNIP1 pLoF, AAF<0.01%	25,715 / 8 / 0	856,988 / 127 / 0	0.008%	3.2 (1.3, 7.8)	0.012
Immune: Nonfamilial Hypogammaglobulinemia					
FNIP1 pLoF, AAF<0.01%	3,751 / 1 / 0	958,365 / 138 / 0	0.007%	4.4 (0.7, 29.5)	0.126
Lung: Bronchiectasis					
FNIP1 pLoF, AAF<0.01%	13,214 / 2 / 0	751,392 / 101 / 0	0.007%	1.5 (0.4, 5.3)	0.531
Lung: Chronic Obstructive Pulmonary Disease					
FNIP1 pLoF, AAF<0.01%	101,028 / 22 / 0	915,911 / 123 / 0	0.007%	2.0 (1.2, 3.4)	0.011
Lung: Interstitial Lung Disease					
FNIP1 pLoF, AAF<0.01%	35,123 / 5 / 0	954,286 / 139 / 0	0.007%	0.9 (0.4, 2.1)	0.742
Muscle: Myopathy					
FNIP1 pLoF, AAF<0.01%	5,089 / 0 / 0	778,308 / 111 / 0	0.007%	0.4 (0.0, 4.8)	0.440

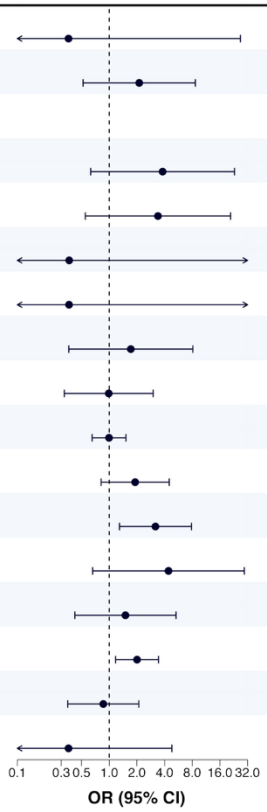

Panel b.

Outcome Gene Variant	Genotype Count RR / RA / AA	AAF	Beta (95% CI) per Allele in Clinical Units	P–Value
CBC: Hematocrit				
FNIP1 pLoF, AAF<0.01%	970,333 / 133 / 0	0.007%	–1.1 (–1.7, –0.4) %	0.002
CBC: Monocyte percentage				
FNIP1 pLoF, AAF<0.01%	874,673 / 120 / 0	0.007%	+0.5 (0.1, 0.9) %	0.023
CBC: Neutrophil Count				
FNIP1 pLoF, AAF<0.01%	897,472 / 127 / 0	0.007%	–0.8 (–1.1, –0.5) K/uL	1.9e–8
ECG: PR interval				
FNIP1 pLoF, AAF<0.01%	225,780 / 25 / 0	0.006%	–10.7 (–19.4, –2.1) ms	0.015
ECG: QRS duration				
FNIP1 pLoF, AAF<0.01%	233,291 / 25 / 0	0.005%	+6.9 (0.6, 13.3) ms	0.033
Immune: Immunoglobulin A				
FNIP1 pLoF, AAF<0.01%	31,277 / 6 / 0	0.010%	+211 (–68, 490) mg/dL	0.139
Immune: Immunoglobulin G				
FNIP1 pLoF, AAF<0.01%	26,194 / 5 / 0	0.010%	–503 (–1266, 259) mg/dL	0.196
Immune: Immunoglobulin M				
FNIP1 pLoF, AAF<0.01%	21,999 / 5 / 0	0.011%	–191 (–475, 94) mg/dL	0.189

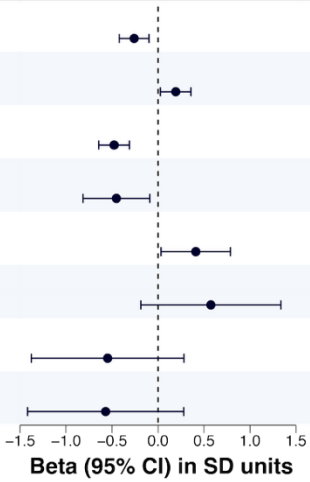

a, Associations of pLOF variants in *FNIP1* with binary traits (OR ± 95% CI), and **b**, quantitative traits (Beta ± 95% CI). Association estimates are from inverse-variance weighted fixed-effect meta-analysis and *P* values are from two-sided Wald tests. AAF, alternative allele frequency; CI, confidence interval; OR, odds ratio; pLOF, predicted loss-of-function; RR, homozygous for the reference allele; RA, heterozygous; AA, homozygous for the alternative allele.

Supplementary Figure 25. Association of variants in *FLCN* with cardiometabolic phenotypes.

Panel a.

Outcome Gene Variant	Genotype Count RR / RA / AA	AAF	Beta (95% CI) per Allele in Clinical Units	P–Value
Triglyceride/HDL Ratio				
FLCN pLoF, AAF<1%	1,031,780 / 336 / 0	0.016%	–0.34 (–0.68, 0.00) ratio	0.051
FLCN plus deleterious missense (5/5 or ESM1vp), AAF<1%	1,028,453 / 3,661 / 2	0.18%	–0.13 (–0.23, –0.02) ratio	0.017
Triglycerides				
FLCN pLoF, AAF<1%	1,075,049 / 349 / 0	0.016%	–11.79 (–21.33, –2.25) mg/dL	0.015
FLCN plus deleterious missense (5/5 or ESM1vp), AAF<1%	1,071,575 / 3,821 / 2	0.18%	–3.63 (–6.52, –0.75) mg/dL	0.014
HDL cholesterol				
FLCN pLoF, AAF<1%	1,032,933 / 336 / 0	0.016%	+0.74 (–0.78, 2.26) mg/dL	0.338
FLCN plus deleterious missense (5/5 or ESM1vp), AAF<1%	1,029,601 / 3,666 / 2	0.18%	+0.39 (–0.07, 0.85) mg/dL	0.096
LDL cholesterol				
FLCN pLoF, AAF<1%	1,067,373 / 347 / 0	0.016%	–2.67 (–6.61, 1.28) mg/dL	0.185
FLCN plus deleterious missense (5/5 or ESM1vp), AAF<1%	1,063,922 / 3,797 / 1	0.18%	+0.17 (–1.02, 1.36) mg/dL	0.777
Non–HDL cholesterol				
FLCN pLoF, AAF<1%	1,032,323 / 334 / 0	0.016%	–4.01 (–8.30, 0.28) mg/dL	0.067
FLCN plus deleterious missense (5/5 or ESM1vp), AAF<1%	1,028,991 / 3,664 / 2	0.18%	–0.56 (–1.85, 0.73) mg/dL	0.399
Apolipoprotein B				
FLCN pLoF, AAF<1%	679,353 / 224 / 0	0.016%	–3.68 (–6.49, –0.87) mg/dL	0.010
FLCN plus deleterious missense (5/5 or ESM1vp), AAF<1%	677,156 / 2,420 / 1	0.18%	–0.48 (–1.33, 0.38) mg/dL	0.273

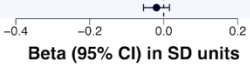

Panel b.

Outcome Gene Variant	Genotype Count RR / RA / AA	AAF	Beta (95% CI) per Allele in Clinical Units	P–Value
(BIA) Body fat mass				
FLCN pLoF, AAF<1%	598,152 / 204 / 0	0.017%	–0.760 (–1.944, 0.424) kg	0.208
FLCN plus deleterious missense (5/5 or ESM1vp), AAF<1%	596,136 / 2,219 / 1	0.19%	–0.333 (–0.695, 0.029) kg	0.071
(BIA) Body fat %				
FLCN pLoF, AAF<1%	598,718 / 205 / 0	0.017%	–1.021 (–2.145, 0.104) %	0.075
FLCN plus deleterious missense (5/5 or ESM1vp), AAF<1%	596,702 / 2,220 / 1	0.19%	–0.343 (–0.688, 0.002) %	0.051
(BIA) Body lean mass				
FLCN pLoF, AAF<1%	582,014 / 201 / 0	0.017%	+0.372 (–0.999, 1.743) kg	0.595
FLCN plus deleterious missense (5/5 or ESM1vp), AAF<1%	580,019 / 2,195 / 1	0.19%	+0.023 (–0.391, 0.438) kg	0.912
(BIA) Body lean %				
FLCN pLoF, AAF<1%	581,999 / 201 / 0	0.017%	+1.062 (–0.070, 2.194) %	0.066
FLCN plus deleterious missense (5/5 or ESM1vp), AAF<1%	580,004 / 2,195 / 1	0.19%	+0.333 (–0.010, 0.677) %	0.057
(MRI) Abdominal to Gluteofemoral Fat Ratio				
FLCN pLoF, AAF<1%	64,292 / 13 / 0	0.010%	–0.051 (–0.152, 0.051) ratio	0.327
FLCN plus deleterious missense (5/5 or ESM1vp), AAF<1%	64,049 / 256 / 0	0.20%	–0.027 (–0.050, –0.004) ratio	0.022
(MRI) Visceral to Gluteofemoral Fat Ratio				
FLCN pLoF, AAF<1%	64,292 / 13 / 0	0.010%	+0.002 (–0.151, 0.155) ratio	0.976
FLCN plus deleterious missense (5/5 or ESM1vp), AAF<1%	64,049 / 256 / 0	0.20%	–0.021 (–0.055, 0.014) ratio	0.245

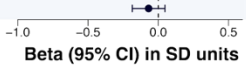

Panel c.

Outcome Gene Variant	Genotype Count RR / RA / AA	AAF	Beta (95% CI) per Allele in Clinical Units	P–Value
Body Mass Index				
FLCN pLoF, AAF<1%	1,236,547 / 416 / 0	0.017%	−0.176 (−0.686, 0.335) kg/m2	0.500
FLCN plus deleterious missense (5/5 or ESM1vp), AAF<1%	1,232,593 / 4,368 / 2	0.18%	−0.110 (−0.269, 0.049) kg/m2	0.172
Waist to Hip Ratio (Adjusted for BMI)				
FLCN pLoF, AAF<1%	620,656 / 215 / 0	0.017%	−0.009 (−0.017, −0.001) ratio	0.031
FLCN plus deleterious missense (5/5 or ESM1vp), AAF<1%	618,570 / 2,300 / 1	0.19%	−0.002 (−0.004, 0.001) ratio	0.123
HbA1c				
FLCN pLoF, AAF<1%	952,264 / 301 / 0	0.016%	−0.132 (−0.237, −0.028) %	0.013
FLCN plus deleterious missense (5/5 or ESM1vp), AAF<1%	949,246 / 3,317 / 2	0.17%	−0.022 (−0.054, 0.009) %	0.166
Random glucose				
FLCN pLoF, AAF<1%	969,380 / 324 / 0	0.017%	−1.482 (−4.203, 1.239) mg/dL	0.286
FLCN plus deleterious missense (5/5 or ESM1vp), AAF<1%	966,091 / 3,611 / 2	0.19%	−0.560 (−1.380, 0.260) mg/dL	0.179
Liver Fat (MRI–PDFF)				
FLCN pLoF, AAF<1%	63,415 / 13 / 0	0.010%	−1.450 (−4.319, 1.420) %	0.322
FLCN plus deleterious missense (5/5 or ESM1vp), AAF<1%	63,176 / 252 / 0	0.20%	−0.349 (−1.002, 0.304) %	0.295
Alanine Aminotransferase				
FLCN pLoF, AAF<1%	905,351 / 295 / 0	0.016%	−1.147 (−2.812, 0.518) U/L	0.177
FLCN plus deleterious missense (5/5 or ESM1vp), AAF<1%	902,252 / 3,392 / 2	0.19%	−0.840 (−1.331, −0.349) U/L	8.1e−4
Aspartate Aminotransferase				
FLCN pLoF, AAF<1%	923,513 / 303 / 0	0.016%	−0.455 (−1.854, 0.943) U/L	0.524
FLCN plus deleterious missense (5/5 or ESM1vp), AAF<1%	920,345 / 3,469 / 2	0.19%	−0.134 (−0.549, 0.280) U/L	0.523
Systolic Blood Pressure				
FLCN pLoF, AAF<1%	1,251,818 / 422 / 0	0.017%	+1.550 (0.043, 3.056) mmHg	0.044
FLCN plus deleterious missense (5/5 or ESM1vp), AAF<1%	1,247,755 / 4,483 / 2	0.18%	+0.482 (0.020, 0.945) mmHg	0.042
Diastolic Blood Pressure				
FLCN pLoF, AAF<1%	1,251,799 / 422 / 0	0.017%	+0.090 (−0.794, 0.974) mmHg	0.842
FLCN plus deleterious missense (5/5 or ESM1vp), AAF<1%	1,247,736 / 4,483 / 2	0.18%	+0.181 (−0.092, 0.453) mmHg	0.194

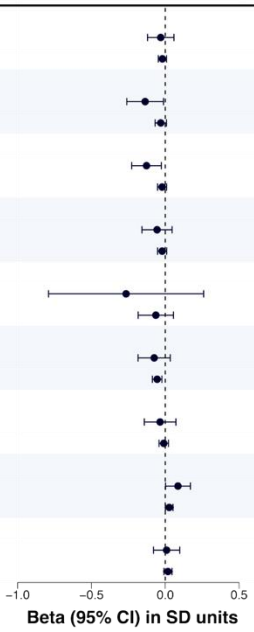

Panel d.

Outcome Gene Variant	Count (Cases) RR / RA / AA	Count (Controls) RR / RA / AA	AAF	Odds Ratio (95% CI) per Allele	P–Value
Coronary Artery Disease					
FLCN pLoF, AAF<1%	88,200 / 34 / 0	625,912 / 212 / 0	0.017%	1.1 (0.8, 1.7)	0.513
FLCN plus deleterious missense (5/5 or ESM1vp), AAF<1%	87,903 / 331 / 0	623,806 / 2,316 / 2	0.19%	1.0 (0.9, 1.1)	0.962
Myocardial Infarction					
FLCN pLoF, AAF<1%	60,956 / 24 / 0	670,637 / 223 / 0	0.017%	1.1 (0.7, 1.8)	0.620
FLCN plus deleterious missense (5/5 or ESM1vp), AAF<1%	60,742 / 238 / 0	668,388 / 2,470 / 2	0.19%	1.0 (0.9, 1.2)	0.766
Type 2 diabetes					
FLCN pLoF, AAF<1%	187,425 / 44 / 0	718,771 / 251 / 0	0.016%	0.7 (0.5, 0.9)	0.014
FLCN plus deleterious missense (5/5 or ESM1vp), AAF<1%	186,874 / 594 / 1	716,393 / 2,628 / 1	0.18%	0.9 (0.8, 1.0)	0.067
Liver Disease (Non Alcoholic)					
FLCN pLoF, AAF<1%	51,677 / 21 / 0	707,792 / 244 / 0	0.017%	1.1 (0.7, 1.9)	0.603
FLCN plus deleterious missense (5/5 or ESM1vp), AAF<1%	51,515 / 183 / 0	705,329 / 2,707 / 0	0.19%	1.0 (0.8, 1.1)	0.623
Liver Cirrhosis (Any)					
FLCN pLoF, AAF<1%	15,252 / 9 / 0	721,587 / 246 / 0	0.017%	2.2 (1.0, 4.9)	0.059
FLCN plus deleterious missense (5/5 or ESM1vp), AAF<1%	15,200 / 61 / 0	719,070 / 2,763 / 0	0.19%	1.2 (0.9, 1.5)	0.286

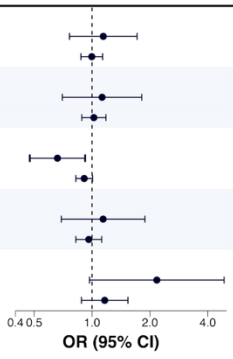

a, Associations of variants in *FLCN* with lipid traits (Beta ± 95% CI), **b**, anthropometric traits (Beta ± 95% CI), **c**, quantitative cardiometabolic traits (Beta ± 95% CI), and **d**, cardiometabolic outcomes (OR ± 95% CI). Association estimates are from inverse-variance weighted fixed-effect meta-analysis and *P* values are from two-sided Wald tests. AAF, alternative allele frequency; CI, confidence interval; ESM1vp, Evolutionary Scale Modeling; OR, odds ratio; pLOF, predicted loss-of-function; RR, homozygous for the reference allele; RA, heterozygous; AA, homozygous for the alternative allele.

Supplementary Figure 26. Association of variants in *FLCN* with Birt–Hogg–Dubé syndrome phenotypes and with risk for liver cancers.

Panel a.

Outcome Gene Variant	Count (Cases) RR / RA / AA	Count (Controls) RR / RA / AA	AAF	Odds Ratio (95% CI) per Allele	P–Value
Endocrine: Parotid Malignancy					
FLCN pLoF, AAF<1%	781 / 1 / 0	503,365 / 147 / 0	0.015%	8.2 (0.7, 92.3)	0.087
FLCN plus deleterious missense (5/5 or ESM1vp), AAF<1%	776 / 6 / 0	501,608 / 1,903 / 1	0.19%	2.5 (1.0, 6.5)	0.059
Endocrine: Thyroid Malignancy					
FLCN pLoF, AAF<1%	7,405 / 1 / 0	559,075 / 161 / 0	0.014%	0.6 (0.1, 2.3)	0.428
FLCN plus deleterious missense (5/5 or ESM1vp), AAF<1%	7,384 / 22 / 0	557,156 / 2,079 / 1	0.19%	0.9 (0.6, 1.3)	0.472
Endocrine: Thyroid Nodule					
FLCN pLoF, AAF<1%	43,943 / 21 / 0	1,002,505 / 335 / 0	0.017%	1.6 (1.0, 2.5)	0.076
FLCN plus deleterious missense (5/5 or ESM1vp), AAF<1%	43,800 / 163 / 1	999,032 / 3,807 / 1	0.19%	1.1 (0.9, 1.3)	0.462
Gastrointestinal: Benign Colon Neoplasm					
FLCN pLoF, AAF<1%	52,961 / 25 / 0	559,075 / 161 / 0	0.015%	2.0 (1.2, 3.2)	0.007
FLCN plus deleterious missense (5/5 or ESM1vp), AAF<1%	52,768 / 218 / 0	557,156 / 2,079 / 1	0.19%	1.1 (0.9, 1.3)	0.300
Gastrointestinal: Colon Malignancy					
FLCN pLoF, AAF<1%	17,532 / 17 / 0	559,075 / 161 / 0	0.015%	4.1 (2.1, 7.8)	1.8e−5
FLCN plus deleterious missense (5/5 or ESM1vp), AAF<1%	17,464 / 85 / 0	557,156 / 2,079 / 1	0.19%	1.3 (1.0, 1.6)	0.047
Gastrointestinal: Colon Polyps					
FLCN pLoF, AAF<1%	115,208 / 45 / 0	951,660 / 317 / 0	0.017%	1.2 (0.9, 1.7)	0.289
FLCN plus deleterious missense (5/5 or ESM1vp), AAF<1%	114,797 / 455 / 1	948,417 / 3,559 / 1	0.19%	1.0 (0.9, 1.2)	0.375
Kidney: Benign Kidney Neoplasm					
FLCN pLoF, AAF<1%	1,554 / 3 / 0	563,394 / 186 / 0	0.017%	7.8 (2.0, 29.9)	0.003
FLCN plus deleterious missense (5/5 or ESM1vp), AAF<1%	1,549 / 8 / 0	561,377 / 2,202 / 1	0.20%	1.6 (0.7, 3.8)	0.261
Kidney: Cystic Kidney Disease					
FLCN pLoF, AAF<1%	5,622 / 3 / 0	981,475 / 325 / 0	0.017%	2.8 (0.6, 14.4)	0.209
FLCN plus deleterious missense (5/5 or ESM1vp), AAF<1%	5,596 / 29 / 0	978,058 / 3,740 / 2	0.19%	1.7 (1.2, 2.6)	0.008
Kidney: Kidney Malgnancy					
FLCN pLoF, AAF<1%	8,858 / 17 / 0	559,075 / 161 / 0	0.016%	9.4 (4.9, 18.0)	2.0e−11
FLCN plus deleterious missense (5/5 or ESM1vp), AAF<1%	8,825 / 50 / 0	557,156 / 2,079 / 1	0.19%	1.7 (1.2, 2.3)	0.002
Lung: Congenital Lung Malformations					
FLCN pLoF, AAF<1%	1,680 / 2 / 0	340,669 / 123 / 0	0.018%	10.4 (2.0, 55.0)	0.006
FLCN plus deleterious missense (5/5 or ESM1vp), AAF<1%	1,673 / 9 / 0	339,458 / 1,333 / 1	0.20%	1.7 (0.8, 3.6)	0.136
Lung: Pneumothorax					
FLCN pLoF, AAF<1%	11,380 / 47 / 0	977,460 / 287 / 0	0.017%	17.8 (11.7, 27.1)	6.3e−41
FLCN plus deleterious missense (5/5 or ESM1vp), AAF<1%	11,338 / 89 / 0	974,027 / 3,718 / 2	0.19%	2.5 (1.9, 3.2)	1.3e−12
Skin Lipomas					
FLCN pLoF, AAF<1%	24,648 / 13 / 0	559,075 / 161 / 0	0.015%	2.4 (1.2, 4.8)	0.012
FLCN plus deleterious missense (5/5 or ESM1vp), AAF<1%	24,568 / 93 / 0	557,156 / 2,079 / 1	0.19%	1.0 (0.8, 1.2)	0.923
Skin: Benign Neoplasm Of Skin					
FLCN pLoF, AAF<1%	86,609 / 42 / 0	878,599 / 288 / 0	0.017%	1.5 (1.0, 2.0)	0.030
FLCN plus deleterious missense (5/5 or ESM1vp), AAF<1%	86,317 / 334 / 0	875,586 / 3,299 / 2	0.19%	1.0 (0.9, 1.1)	0.931
Skin: Diseases of Sebaceous Glands					
FLCN pLoF, AAF<1%	76,818 / 43 / 0	853,433 / 263 / 0	0.016%	2.0 (1.4, 2.9)	2.0e−4
FLCN plus deleterious missense (5/5 or ESM1vp), AAF<1%	76,524 / 337 / 0	850,554 / 3,141 / 1	0.19%	1.2 (1.1, 1.4)	5.7e−4
Skin: Melanoma					
FLCN pLoF, AAF<1%	14,967 / 9 / 0	559,075 / 161 / 0	0.015%	2.1 (0.9, 4.9)	0.073
FLCN plus deleterious missense (5/5 or ESM1vp), AAF<1%	14,897 / 79 / 0	557,156 / 2,079 / 1	0.19%	1.3 (1.0, 1.7)	0.026
Skin: Sebaceous Cyst					
FLCN pLoF, AAF<1%	44,665 / 29 / 0	850,119 / 261 / 0	0.016%	2.6 (1.7, 4.0)	1.7e−5
FLCN plus deleterious missense (5/5 or ESM1vp), AAF<1%	44,487 / 207 / 0	847,250 / 3,129 / 1	0.19%	1.3 (1.1, 1.5)	9.1e−4

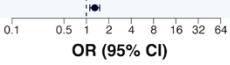

Panel b.

Outcome Gene Variant	Count (Cases) RR / RA / AA	Count (Controls) RR / RA / AA	AAF	Odds Ratio (95% CI) per Allele	P–Value
Gastrointestinal: Hepatocellular or Cholangio Carcinomas					
FNIP1 pLoF, AAF<1%	3,974 / 1 / 0	559,160 / 76 / 0	0.007%	0.8 (0.1, 6.7)	0.874
FLCN pLoF, AAF<1%	3,974 / 1 / 0	559,075 / 161 / 0	0.014%	2.0 (0.4, 10.1)	0.393
FLCN plus deleterious missense (5/5 or ESM1vp), AAF<1%	3,962 / 13 / 0	557,156 / 2,079 / 1	0.19%	0.9 (0.5, 1.6)	0.766

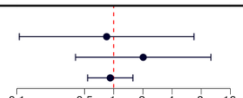

a, Associations of *FLCN* variants (i.e. pLOF or pLOF plus deleterious missense) with Birt–Hogg–Dubé syndrome phenotypes (OR ± 95% CI). **b**, Associations of *FLCN* variants with a composite phenotype of hepatocellular carcinoma and cholangiocarcinoma (OR ± 95% CI); *FNIP1* associations are shown for comparison in this panel. Association estimates are from inverse-variance weighted fixed-effect meta-analysis and *P* values are from two-sided Wald tests. AAF, alternative allele frequency; CI, confidence interval; ESM1vp, Evolutionary Scale Modeling; OR, odds ratio; pLOF, predicted loss-of-function; RR, homozygous for the reference allele; RA, heterozygous; AA, homozygous for the alternative allele**.**

Supplementary Figure 27. Association of variants in *FNIP2* with cardiometabolic phenotypes.

Panel a.

Outcome Gene Variant	Genotype Count RR / RA / AA	AAF	Beta (95% CI) per Allele in Clinical Units	P–Value
Triglyceride/HDL Ratio				
FNIP2 pLoF, AAF<1%	1,026,821 / 149 / 0	0.007%	–0.1 (–0.6, 0.4) ratio	0.669
FNIP2 pLoF plus deleterious missense (ESM1vp), AAF<1%	1,026,768 / 202 / 0	0.010%	–0.2 (–0.6, 0.3) ratio	0.409
Triglycerides				
FNIP2 pLoF, AAF<1%	1,070,030 / 154 / 0	0.007%	+0.5 (–13.9, 14.9) mg/dL	0.944
FNIP2 pLoF plus deleterious missense (ESM1vp), AAF<1%	1,069,977 / 207 / 0	0.010%	–1.1 (–13.5, 11.4) mg/dL	0.867
HDL cholesterol				
FNIP2 pLoF, AAF<1%	1,027,964 / 149 / 0	0.007%	+2.5 (0.2, 4.8) mg/dL	0.032
FNIP2 pLoF plus deleterious missense (ESM1vp), AAF<1%	1,027,911 / 202 / 0	0.010%	+2.8 (0.8, 4.8) mg/dL	0.005
LDL cholesterol				
FNIP2 pLoF, AAF<1%	1,062,453 / 153 / 0	0.007%	+8.1 (2.1, 14.0) mg/dL	0.008
FNIP2 pLoF plus deleterious missense (ESM1vp), AAF<1%	1,062,400 / 206 / 0	0.010%	+7.7 (2.6, 12.9) mg/dL	0.003
Non–HDL cholesterol				
FNIP2 pLoF, AAF<1%	1,027,364 / 149 / 0	0.007%	+7.2 (0.8, 13.6) mg/dL	0.028
FNIP2 pLoF plus deleterious missense (ESM1vp), AAF<1%	1,027,311 / 202 / 0	0.010%	+7.3 (1.7, 12.8) mg/dL	0.010
Apolipoprotein B				
FNIP2 pLoF, AAF<1%	652,898 / 80 / 0	0.006%	+6.4 (1.7, 11.1) mg/dL	0.008
FNIP2 pLoF plus deleterious missense (ESM1vp), AAF<1%	652,863 / 115 / 0	0.009%	+5.3 (1.3, 9.3) mg/dL	0.009

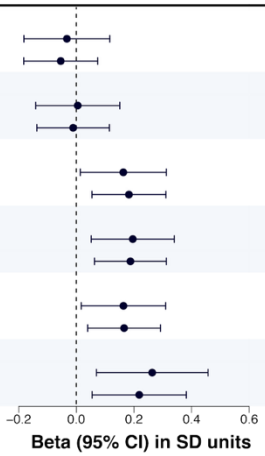

Panel b.

Outcome Gene Variant	Genotype Count RR / RA / AA	AAF	Beta (95% CI) per Allele in Clinical Units	P–Value
(BIA) Body fat mass				
FNIP2 pLoF, AAF<1%	598,282 / 74 / 0	0.006%	–0.150 (–2.111, 1.811) kg	0.881
FNIP2 pLoF plus deleterious missense (ESM1vp), AAF<1%	598,264 / 92 / 0	0.008%	–0.028 (–1.779, 1.723) kg	0.975
(BIA) Body fat %				
FNIP2 pLoF, AAF<1%	598,848 / 74 / 0	0.006%	+0.235 (–2.992, 3.463) %	0.886
FNIP2 pLoF plus deleterious missense (ESM1vp), AAF<1%	598,830 / 92 / 0	0.008%	+0.176 (–4.752, 5.104) %	0.944
(BIA) Body lean mass				
FNIP2 pLoF, AAF<1%	582,141 / 74 / 0	0.006%	–1.494 (–3.742, 0.753) kg	0.193
FNIP2 pLoF plus deleterious missense (ESM1vp), AAF<1%	582,127 / 88 / 0	0.008%	–1.401 (–3.463, 0.660) kg	0.183
(BIA) Body lean %				
FNIP2 pLoF, AAF<1%	582,126 / 74 / 0	0.006%	–0.319 (–2.179, 1.541) %	0.737
FNIP2 pLoF plus deleterious missense (ESM1vp), AAF<1%	582,112 / 88 / 0	0.008%	+0.056 (–1.650, 1.761) %	0.949
(MRI) Abdominal to Gluteofemoral Fat Ratio				
FNIP2 pLoF, AAF<1%	64,301 / 4 / 0	0.003%	+0.040 (–0.143, 0.223) ratio	0.667
FNIP2 pLoF plus deleterious missense (ESM1vp), AAF<1%	64,299 / 6 / 0	0.005%	+0.030 (–0.119, 0.179) ratio	0.693
(MRI) Visceral to Gluteofemoral Fat Ratio				
FNIP2 pLoF, AAF<1%	64,301 / 4 / 0	0.003%	–0.021 (–0.297, 0.255) ratio	0.880
FNIP2 pLoF plus deleterious missense (ESM1vp), AAF<1%	64,299 / 6 / 0	0.005%	+0.000 (–0.225, 0.225) ratio	1.000

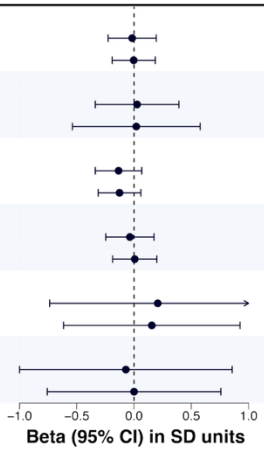

Panel c.

Outcome Gene Variant	Genotype Count RR / RA / AA	AAF	Beta (95% CI) per Allele in Clinical Units	P–Value
Body Mass Index				
FNIP2 pLoF, AAF<1%	1,236,789 / 174 / 0	0.007%	−0.238 (−1.029, 0.553) kg/m2	0.557
FNIP2 pLoF plus deleterious missense (ESM1vp), AAF<1%	1,236,729 / 234 / 0	0.009%	−0.259 (−0.941, 0.422) kg/m2	0.456
Waist to Hip Ratio (Adjusted for BMI)				
FNIP2 pLoF, AAF<1%	620,795 / 76 / 0	0.006%	−0.003 (−0.017, 0.010) ratio	0.605
FNIP2 pLoF plus deleterious missense (ESM1vp), AAF<1%	620,777 / 94 / 0	0.008%	−0.004 (−0.016, 0.007) ratio	0.461
HbA1c				
FNIP2 pLoF, AAF<1%	947,225 / 136 / 0	0.007%	−0.042 (−0.197, 0.112) %	0.591
FNIP2 pLoF plus deleterious missense (ESM1vp), AAF<1%	947,181 / 180 / 0	0.010%	−0.089 (−0.223, 0.045) %	0.194
Random glucose				
FNIP2 pLoF, AAF<1%	964,352 / 140 / 0	0.007%	−0.115 (−4.230, 4.001) mg/dL	0.957
FNIP2 pLoF plus deleterious missense (ESM1vp), AAF<1%	964,319 / 173 / 0	0.009%	−0.269 (−3.967, 3.429) mg/dL	0.886
Liver Fat (MRI–PDFF)				
FNIP2 pLoF, AAF<1%	63,424 / 4 / 0	0.003%	−0.096 (−5.271, 5.078) %	0.971
FNIP2 pLoF plus deleterious missense (ESM1vp), AAF<1%	63,422 / 6 / 0	0.005%	+1.244 (−2.981, 5.469) %	0.564
Alanine Aminotransferase				
FNIP2 pLoF, AAF<1%	905,514 / 131 / 0	0.007%	−2.176 (−4.676, 0.325) U/L	0.088
FNIP2 pLoF plus deleterious missense (ESM1vp), AAF<1%	905,484 / 161 / 0	0.009%	−2.509 (−4.764, −0.254) U/L	0.029
Aspartate Aminotransferase				
FNIP2 pLoF, AAF<1%	923,683 / 132 / 0	0.007%	−2.139 (−4.264, −0.015) U/L	0.048
FNIP2 pLoF plus deleterious missense (ESM1vp), AAF<1%	923,653 / 162 / 0	0.009%	−2.686 (−4.603, −0.768) U/L	0.006
Systolic Blood Pressure				
FNIP2 pLoF, AAF<1%	1,252,063 / 177 / 0	0.007%	−1.204 (−3.518, 1.110) mmHg	0.308
FNIP2 pLoF plus deleterious missense (ESM1vp), AAF<1%	1,252,005 / 235 / 0	0.009%	−1.346 (−3.357, 0.664) mmHg	0.190
Diastolic Blood Pressure				
FNIP2 pLoF, AAF<1%	1,252,044 / 177 / 0	0.007%	−0.252 (−1.611, 1.107) mmHg	0.716
FNIP2 pLoF plus deleterious missense (ESM1vp), AAF<1%	1,251,986 / 235 / 0	0.009%	−0.305 (−1.487, 0.877) mmHg	0.613

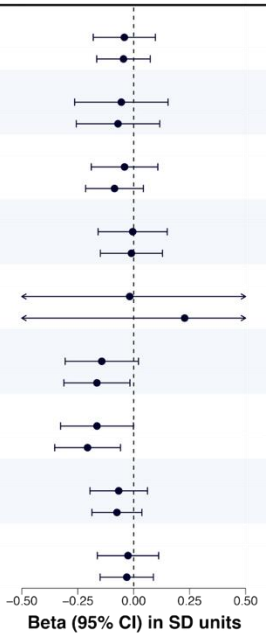

Panel d.

Outcome Gene Variant	Count (Cases) RR / RA / AA	Count (Controls) RR / RA / AA	AAF	Odds Ratio (95% CI) per Allele	P–Value
Coronary Artery Disease					
FNIP2 pLoF, AAF<1%	88,230 / 4 / 0	626,028 / 96 / 0	0.007%	0.5 (0.2, 1.0)	0.044
FNIP2 pLoF plus deleterious missense (ESM1vp), AAF<1%	88,227 / 7 / 0	626,003 / 121 / 0	0.009%	0.5 (0.3, 1.0)	0.058
Myocardial Infarction					
FNIP2 pLoF, AAF<1%	60,979 / 1 / 0	670,757 / 103 / 0	0.007%	0.3 (0.2, 0.8)	0.010
FNIP2 pLoF plus deleterious missense (ESM1vp), AAF<1%	60,977 / 3 / 0	670,732 / 128 / 0	0.009%	0.4 (0.2, 0.8)	0.014
Type 2 diabetes					
FNIP2 pLoF, AAF<1%	187,446 / 23 / 0	718,928 / 94 / 0	0.006%	0.9 (0.5, 1.5)	0.646
FNIP2 pLoF plus deleterious missense (ESM1vp), AAF<1%	187,438 / 31 / 0	718,892 / 130 / 0	0.009%	0.8 (0.5, 1.2)	0.285
Liver Disease (Non Alcoholic)					
FNIP2 pLoF, AAF<1%	51,690 / 8 / 0	707,934 / 102 / 0	0.007%	0.7 (0.4, 1.5)	0.405
FNIP2 pLoF plus deleterious missense (ESM1vp), AAF<1%	51,689 / 9 / 0	707,909 / 127 / 0	0.009%	0.7 (0.4, 1.4)	0.329
Liver Cirrhosis (Any)					
FNIP2 pLoF, AAF<1%	15,260 / 1 / 0	721,729 / 104 / 0	0.007%	0.5 (0.1, 1.7)	0.264
FNIP2 pLoF plus deleterious missense (ESM1vp), AAF<1%	15,260 / 1 / 0	721,704 / 129 / 0	0.009%	0.5 (0.1, 1.4)	0.174

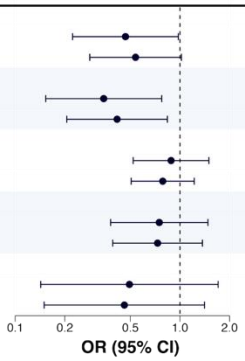

a, Associations of variants in *FNIP2* with lipid traits (Beta ± 95% CI), **b**, anthropometric traits (Beta ± 95% CI), **c**, quantitative cardiometabolic traits (Beta ± 95% CI), and **d**, cardiometabolic outcomes (OR ± 95% CI). Association estimates are from inverse-variance weighted fixed-effect meta-analysis and *P* values are from two-sided Wald tests. AAF, alternative allele frequency; CI, confidence interval; ESM1vp, Evolutionary Scale Modeling; OR, odds ratio; pLOF, predicted loss-of-function; RR, homozygous for the reference allele; RA, heterozygous; AA, homozygous for the alternative allele.

Supplementary Figure 28. Single cell RNA expression plots of *FLCN*, *FNIP1* and *FNIP2* in human and mouse liver.

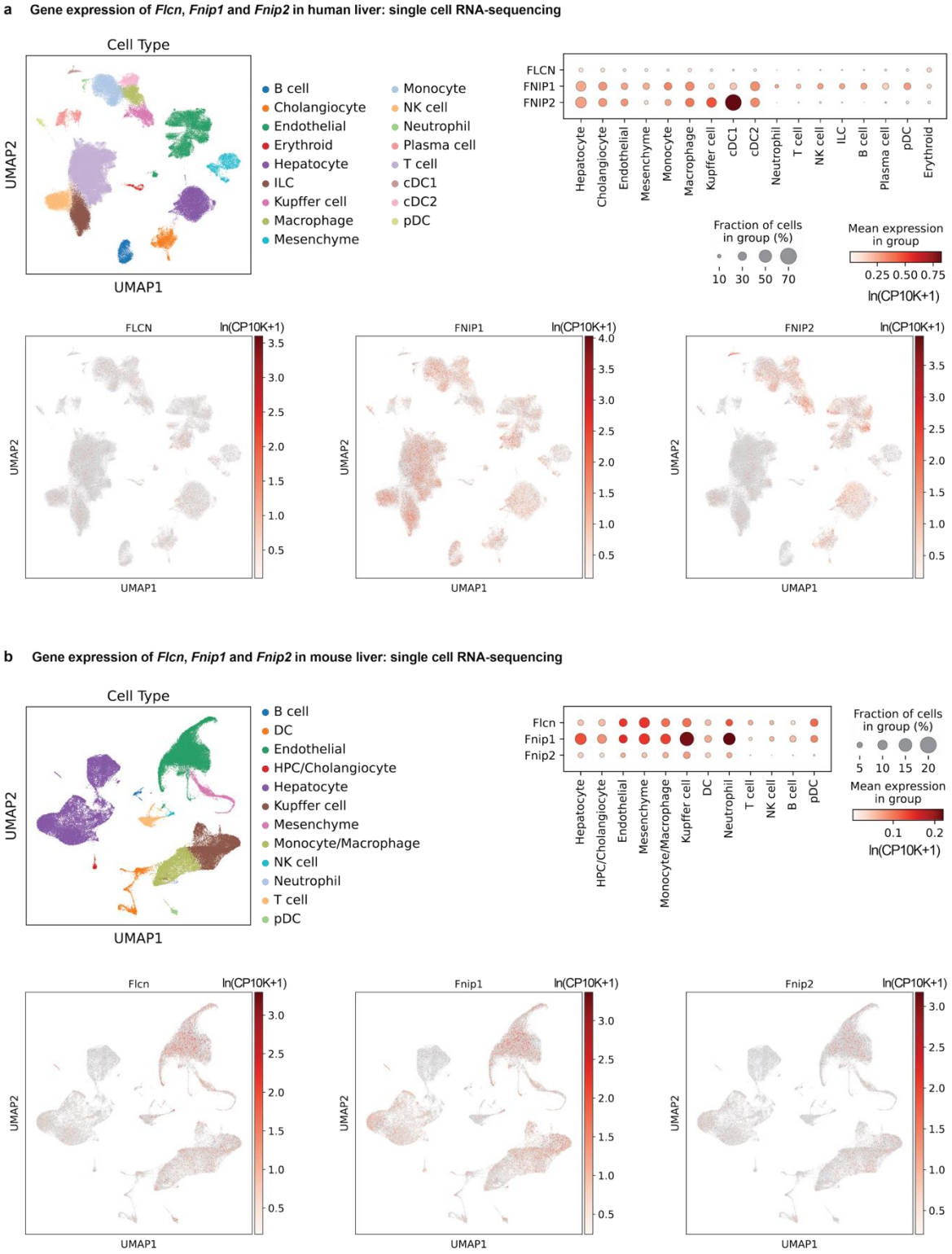

a, Expression of *FLCN*, *FNIP1*, and *FNIP2* in human liver single cell data generated by integrating 5 published datasets (See Methods) with healthy and cirrhosis liver samples. (top left), UMAP of integrated human liver single cell data, colored by unsupervised major cell type clusters. (top right), dot plot of average expression of each gene in each cell type. Color gradient indicates mean expression and spot size indicates percent of cells with non-zero expression. (bottom), expression of each gene projected onto a UMAP, colored by magnitude of expression. Cells with zero expression are shown in grey. **b**, Expression of *Flcn*, *Fnip1*, and *Fnip2* in published mouse liver single cell data containing chow-fed and high fat, high fructose diet-fed mice (See Methods). (top left), UMAP of mouse liver single cell data, colored by unsupervised major cell type clusters. (top right), dot plot of average expression of each gene in each cell type. Color gradient indicates mean expression and spot size indicates percent of cells with non-zero expression. (bottom), expression of each gene projected onto a UMAP, colored by magnitude of expression. Cells with zero expression are shown in grey. UMAP, uniform manifold approximation projection; CP10K, counts per 10,000; ILC, innate lymphoid cell; NK, natural killer; cDC1, conventional dendritic cell 1; cDC2, conventional dendritic cell 2; pDC, plasmacytoid dendritic cell; HPC, hepatic progenitor cell.

Supplementary Figure 29. AAV8 does not perturb FLCN/FNIP in extrahepatic tissues.

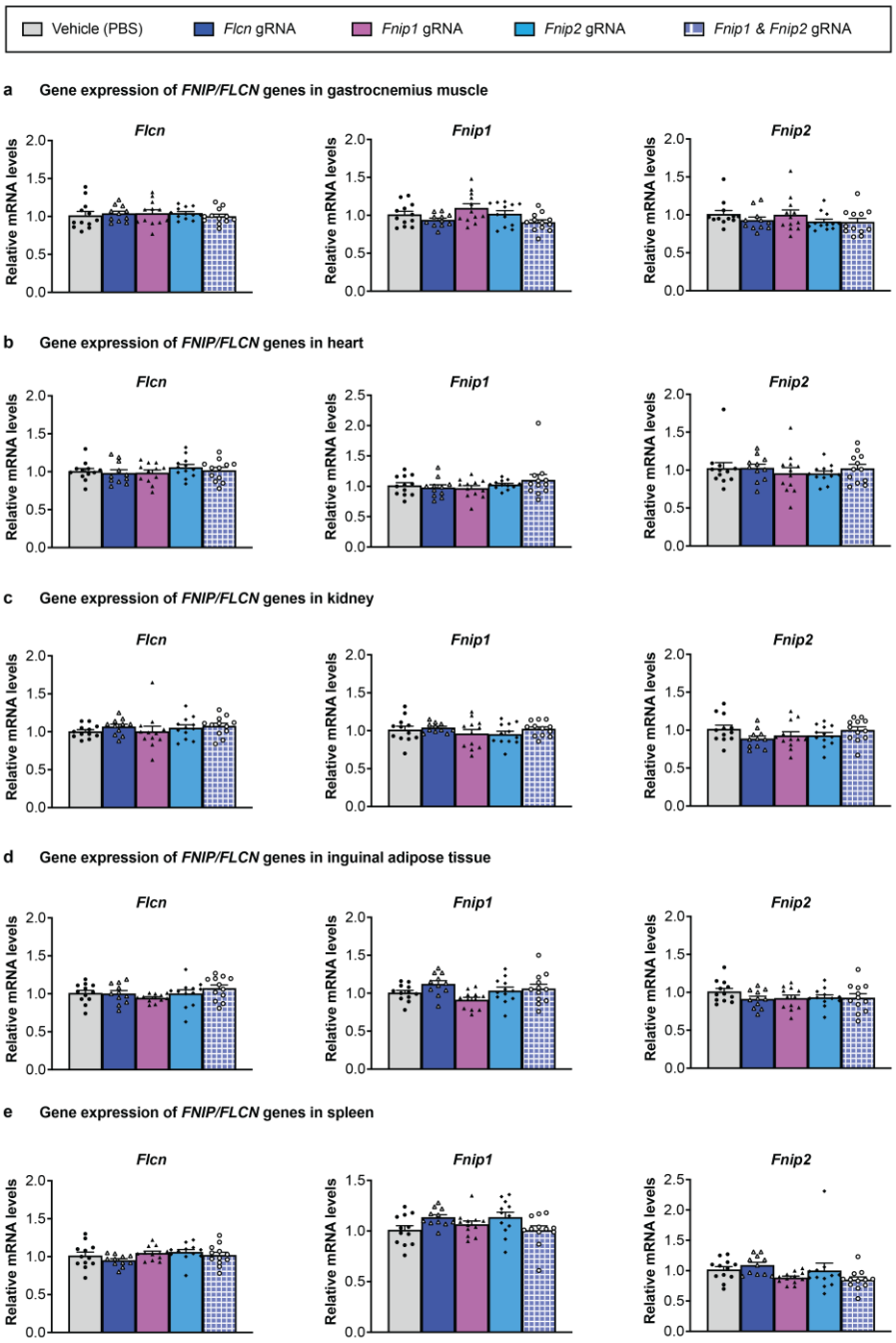

Male *Cas9-Ready* mice were challenged with high fat, high fructose diet for 13 weeks. **a-e,** mRNA levels of *Flcn*, *Fnip1* and *Fnip2* in gastrocnemius muscle (**a**), heart (**b**), kidney (**c**), inguinal adipose tissue (**d**) and spleen (**e**). For all mRNA levels, mean ± s.e.m. are shown. Data are from n = 12 (vehicle control), n = 11 (*Flcn* gRNA), n = 12 (*Fnip1* gRNA), n = 12 (*Fnip2* gRNA) and n = 12 (*Fnip1* & *Fnip2* gRNAs) biologically independent mice. Statistical analysis was performed using one-way ANOVA with Dunnett's correction posttest relative to vehicle control. See also Source Data.

Supplementary Figure 30. *Flcn* or *Fnip1* & Fnip2 inhibition in liver of *Cas9-Ready* mice protects against diet-induced metabolic disease at thermoneutrality.

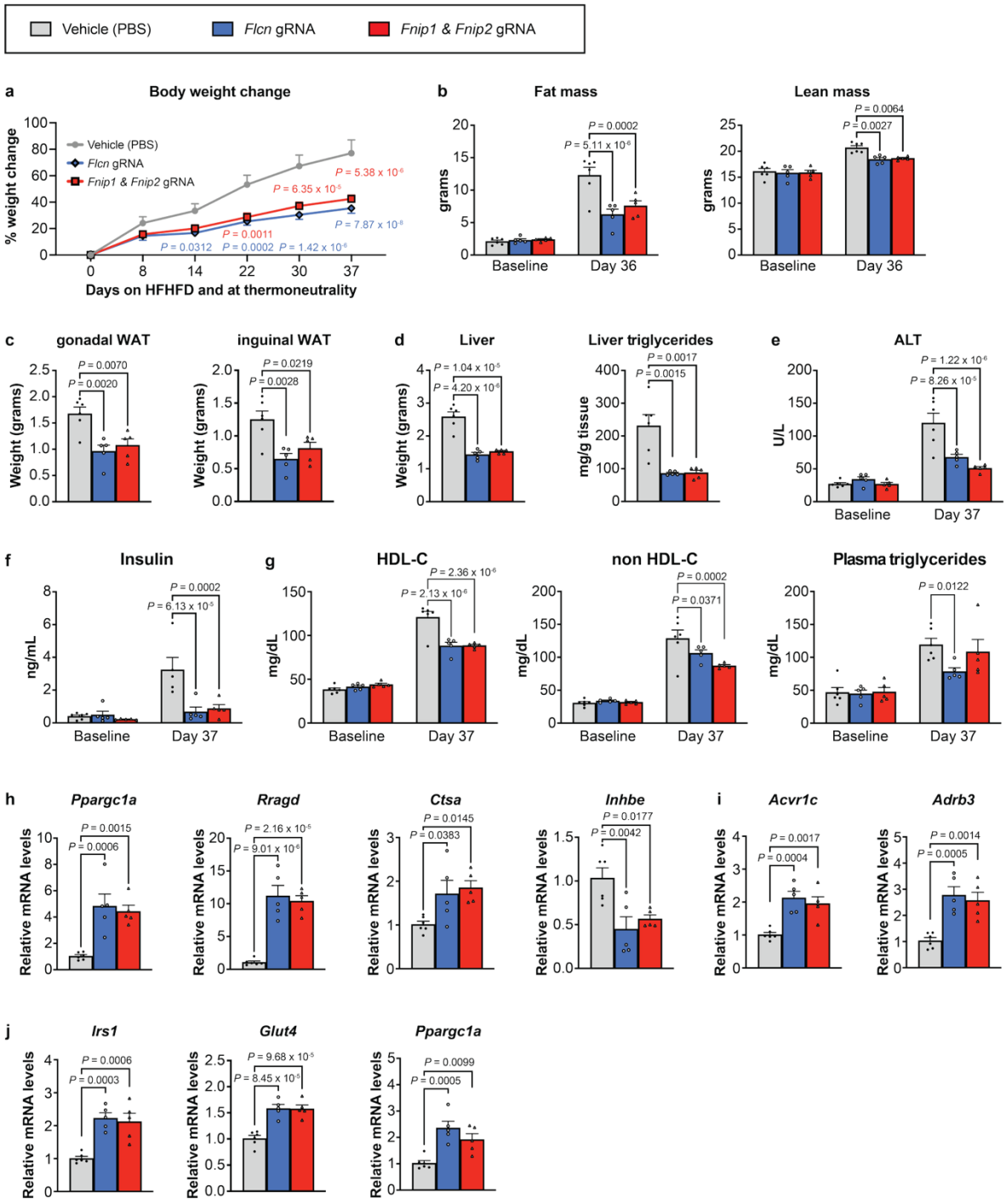

Male *Cas9-Ready* mice were challenged with high fat, high fructose diet and housed at thermoneutral conditions (30°C) for 37 days. **a**, Body weight % change of 6–11 week old male AAV8-gRNA or vehicle (PBS)-treated *Cas9-Ready* mice. Mean ± s.e.m. are shown. *P* values are from two-way ANOVA with Dunnett's correction posttest relative

to vehicle control. **b**, Fat and lean mass was determined by echoMRI at baseline and 36 days post-AAV-gRNA administration. Mean ± s.e.m. are shown. *P* values are from two-way ANOVA with Dunnett's correction posttest relative to vehicle control. **c**, Adipose tissue weights at day 37. Mean ± s.e.m. are shown. *P* values are from one-way ANOVA with Dunnett's correction posttest relative to vehicle control. **d**, Liver weights and liver triglyceride content at Day 37. Mean ± s.e.m. are shown. *P* values are from one-way ANOVA with Dunnett's correction posttest relative to vehicle control. **e-g**, Plasma ALT (**e**), insulin (**f**) and lipid levels (**g**) were determined at baseline and 37 days after housing at thermoneutral conditions while challenged with high fat, high fructose diet. Mean ± s.e.m. are shown. *P* values are from two-way ANOVA with Dunnett's correction posttest relative to vehicle control. **h**, mRNA levels measured at day 37 in liver. **i-j**, mRNA levels measured at day 37 in gonadal adipose tissue showing genes related to lipolysis (**i**) and energy metabolism (**j**). For all mRNA levels, mean ± s.e.m. are shown. *P* values are from one-way ANOVA with Dunnett's correction posttest relative to vehicle control. For all measurements, data are from n = 6 (vehicle control), n = 5 (*Flcn* gRNA), and n = 5 (*Fnip1* & *Fnip2* gRNAs) biologically independent mice, and exact *P* values are shown in the corresponding panels. See also Source Data.

Supplementary Figure 31. *Flcn* or *Fnip1* & *Fnip2* inhibition in liver of *Cas9-Ready* mice lowers weight gain and liver fat accumulation on chow diet.

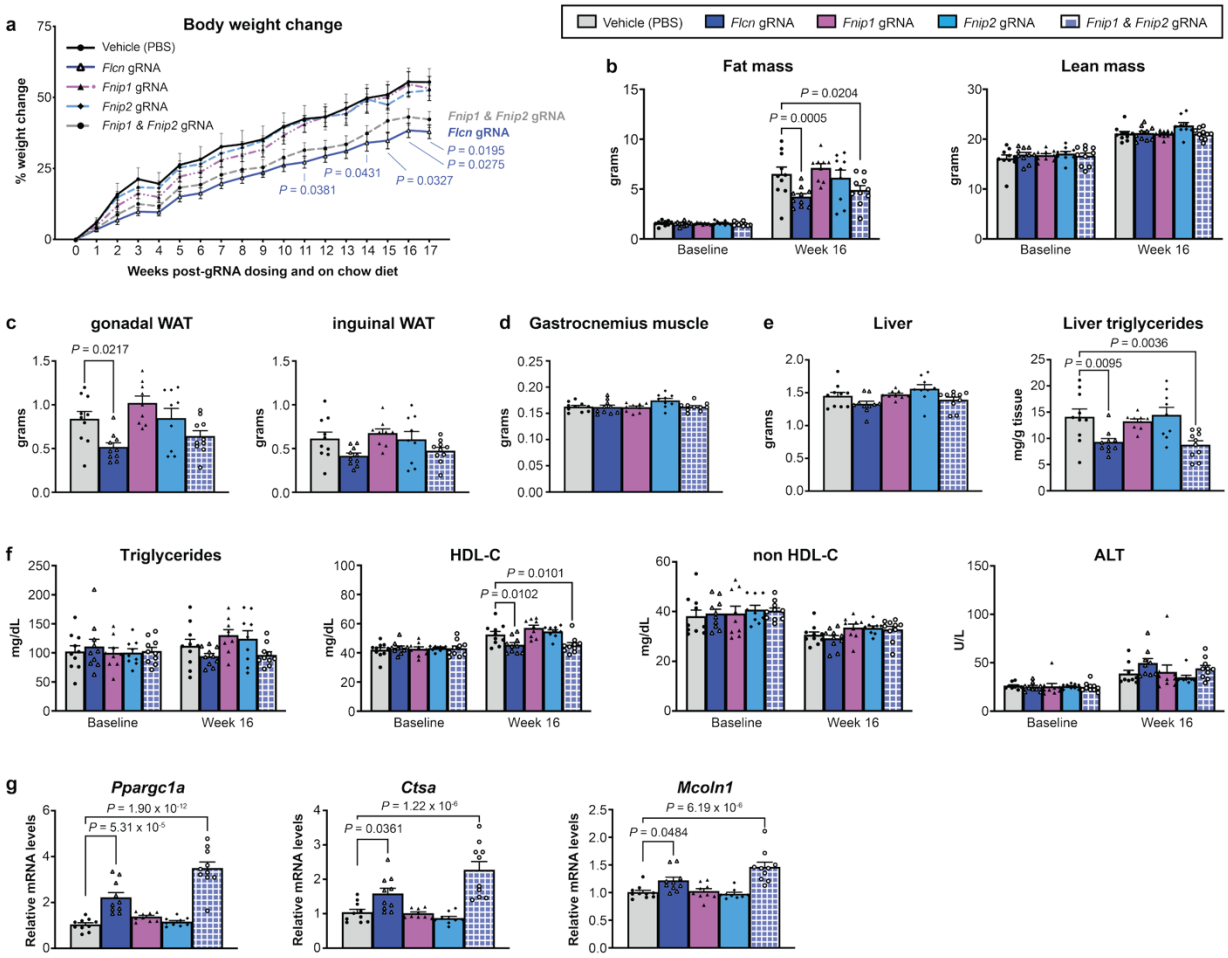

Male *Cas9-Ready* mice were monitored on chow diet for 17 weeks. **a**, Body weight % change of 7–24 week old male AAV8-gRNA or vehicle (PBS)-treated *Cas9-Ready* mice. Mean ± s.e.m. are shown. *P* values are from two-way ANOVA with Dunnett's correction posttest relative to vehicle control. **b**, Fat and lean mass were determined by echoMRI at baseline and 16 weeks post-AAV-gRNA administration. Mean ± s.e.m. are shown. *P* values are from two-way ANOVA with Dunnett's correction posttest relative to vehicle control. **c**, Adipose tissue weights at week 17. Mean ± s.e.m. are shown. *P* values are from one-way ANOVA with Dunnett's correction posttest relative to vehicle control. **d**, Gastrocnemius muscle weights at week 17. Mean ± s.e.m. are shown. *P* values are from one-way ANOVA with Dunnett's correction posttest relative to vehicle control. **e**, Liver weights and liver triglyceride content at week 17. Mean ± s.e.m. are shown. *P* values are from one-way ANOVA with Dunnett's correction posttest relative to vehicle control. **f**, Plasma triglycerides, HDL-C, non HDL-C and ALT levels were determined at baseline and 16 weeks post-AAV-gRNA administration on chow diet. Mean ± s.e.m. are shown. *P* values are from two-way ANOVA with Dunnett's correction posttest relative to vehicle control. **g**, Hepatic mRNA levels measured at week 17 showing genes related to mitochondrial and lysosomal function. Mean ± s.e.m. are shown. *P* values are from one-way ANOVA with Dunnett's correction posttest relative to vehicle control. For all measurements, data are from n = 10 (vehicle control), n = 10 (*Flcn* gRNA), n = 9 (*Fnip1* gRNA), n = 9 (*Fnip2* gRNA) and n = 10 (*Fnip1* & *Fnip2* gRNAs) biologically independent mice, and exact *P* values are shown in the corresponding panels. See also Source Data.

Supplementary Figure 32. *HPN* gene expression across tissues. Data are from the GTEx resource.

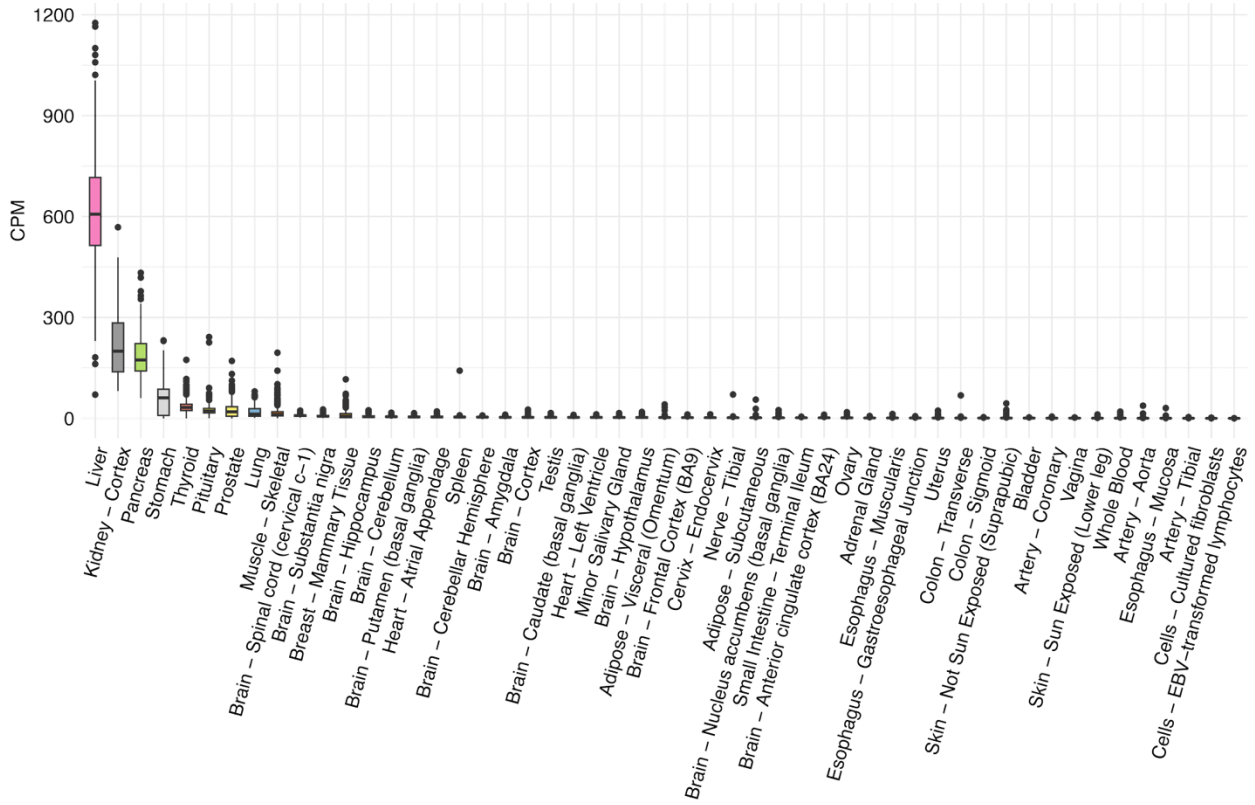

Supplementary Figure 33. Hepatic *Hpn* inhibition lowers plasma cholesterol and protein levels.

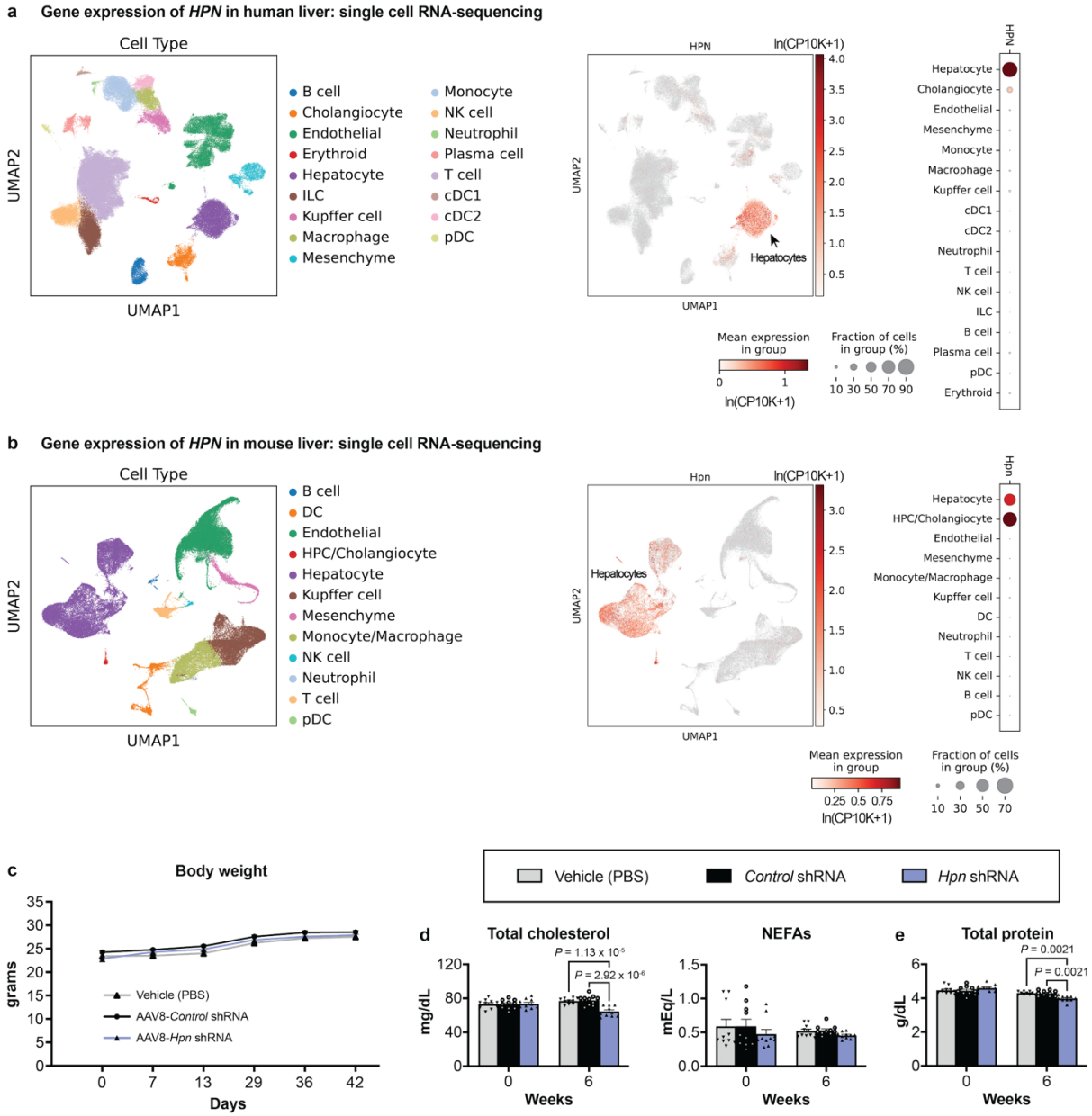

a, Expression of *HPN* in human liver single cell data generated by integrating 5 published datasets (See Methods) with healthy and cirrhosis liver samples. (left), UMAP of integrated human liver single cell data, colored by unsupervised major cell type clusters. (middle), expression of *HPN* projected onto a UMAP, colored by magnitude of expression. Cells with zero expression are shown in grey. (right), dot plot of average *HPN* expression in each cell type. Color gradient indicates mean expression and spot size indicates percent of cells with non-zero expression. **b**, Expression of *Hpn* in published mouse liver single cell data containing chow-fed and high fat, high fructose diet (HFHFD)-fed mice (See Methods). (left), UMAP of integrated mouse liver single cell data, colored by unsupervised major cell type clusters. (middle), expression of *Hpn* projected onto a UMAP, colored by magnitude of expression. Cells with zero expression are shown in grey. (right), dot plot of average *Hpn* expression in each cell type. Color

gradient indicates mean expression and spot size indicates percent of cells with non-zero expression. UMAP, uniform manifold approximation projection; CP10K, counts per 10,000; ILC, innate lymphoid cell; NK, natural killer; cDC1, conventional dendritic cell 1; cDC2, conventional dendritic cell 2; pDC, plasmacytoid dendritic cell; HPC, hepatic progenitor cell. **c**, Body weights of 7–12 week old male AAV8-*Control* shRNA, AAV8-*Hpn* shRNA or vehicle (PBS)-treated WT mice on standard diet (n = 10). **d**, Non-fasted plasma cholesterol and non-esterified fatty acids (NEFAs) of WT mice before (week 0) and 6 weeks after AAV-shRNA or vehicle administration. **e**, Non-fasted plasma total protein levels of WT mice before (week 0) and 6 weeks after AAV-shRNA or vehicle administration. For all measurements, mean ± s.e.m. are shown (n = 10 mice per group). *P* values are from two-way ANOVA with Tukey correction posttest relative to vehicle or control shRNA. In **d-e**, exact *P* values are shown in the corresponding panels. See also Source Data.

Supplementary Figure 34. Regional plot for the associations of common variants at the *HPN* locus.

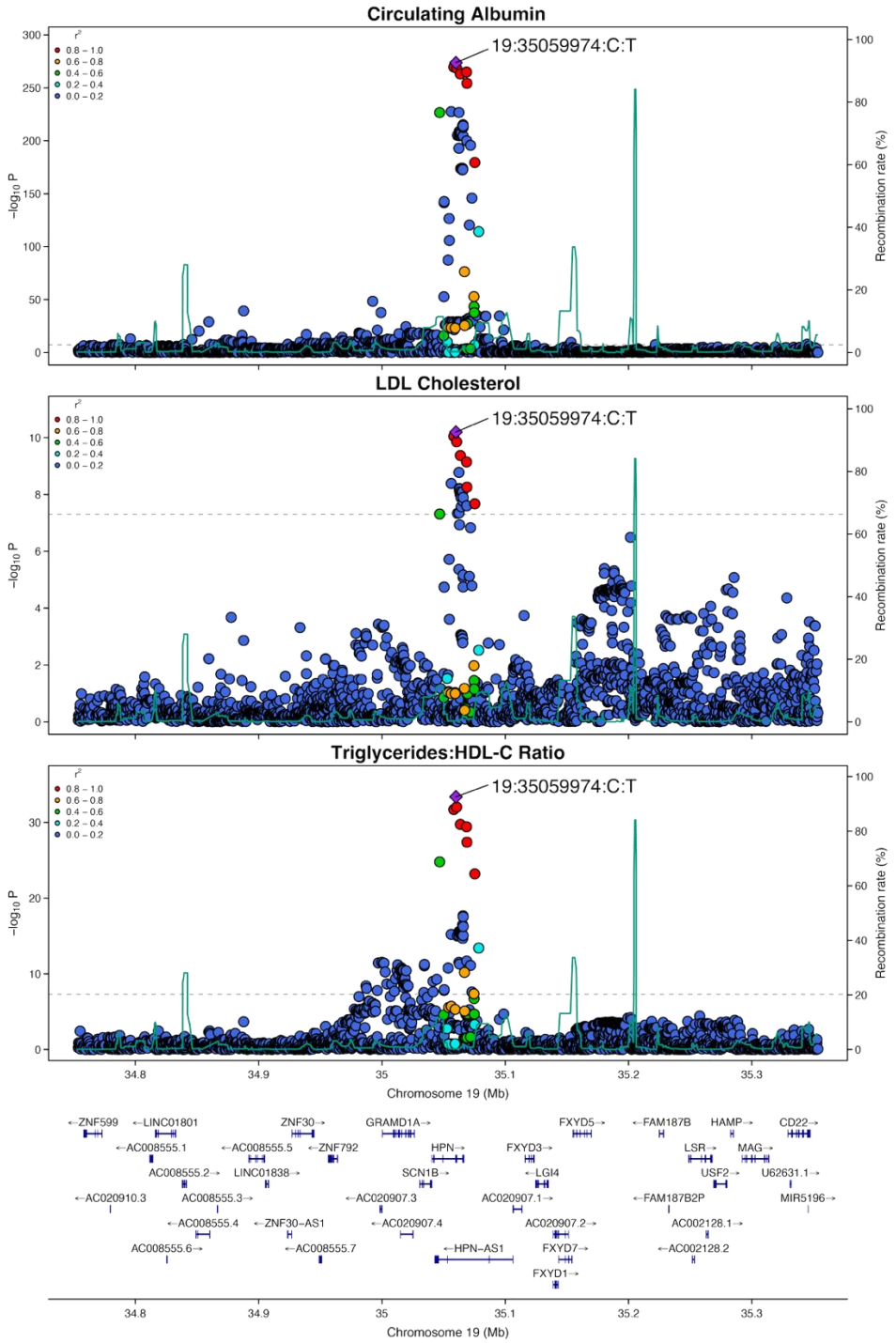

Supplementary Figure 35. Genetic associations for *HPN* common and rare variants.

Panel a.

Outcome Gene Variant	Genotype Count RR / RA / AA	AAF	Beta (95% CI) per Allele in Clinical Units	P–Value
(BIA) Body fat mass				
HPN pLoF, AAF<1%	569,565 / 31 / 0	0.003%	+0.091 (–2.843, 3.026) kg	0.952
HPN pLoF plus deleterious missense (5/5 or ESM1vp), AAF<0.1%	597,374 / 981 / 1	0.082%	–0.232 (–0.775, 0.311) kg	0.401
rs45512696 – *HPN* expression raising allele (T)	426,983 / 156,024 / 15,336	15.6%	+0.012 (–0.032, 0.056) kg	0.589
(BIA) Body fat %				
HPN pLoF, AAF<1%	570,129 / 31 / 0	0.003%	–0.452 (–3.203, 2.299) %	0.748
HPN pLoF plus deleterious missense (5/5 or ESM1vp), AAF<0.1%	597,941 / 981 / 1	0.082%	–0.290 (–0.804, 0.223) %	0.268
rs45512696 – *HPN* expression raising allele (T)	427,396 / 156,166 / 15,348	15.6%	+0.050 (0.009, 0.090) %	0.016
(BIA) Body lean mass				
HPN pLoF, AAF<1%	553,424 / 31 / 0	0.003%	+1.403 (–2.073, 4.878) kg	0.429
HPN pLoF plus deleterious missense (5/5 or ESM1vp), AAF<0.1%	581,247 / 967 / 1	0.083%	+0.194 (–0.429, 0.816) kg	0.542
rs45512696 – *HPN* expression raising allele (T)	414,123 / 152,916 / 15,165	15.7%	–0.113 (–0.163, –0.063) kg	8.0e–6
(BIA) Body lean %				
HPN pLoF, AAF<1%	553,409 / 31 / 0	0.003%	+0.518 (–2.326, 3.363) %	0.721
HPN pLoF plus deleterious missense (5/5 or ESM1vp), AAF<0.1%	581,232 / 967 / 1	0.083%	+0.270 (–0.247, 0.786) %	0.305
rs45512696 – *HPN* expression raising allele (T)	414,111 / 152,913 / 15,165	15.7%	–0.050 (–0.092, –0.009) %	0.016
(MRI) Abdominal to Gluteofemoral Fat Ratio				
HPN pLoF, AAF<1%	64,304 / 1 / 0	0.0008%	+0.129 (–0.237, 0.494) ratio	0.490
HPN pLoF plus deleterious missense (5/5 or ESM1vp), AAF<0.1%	64,188 / 117 / 0	0.091%	–0.011 (–0.045, 0.023) ratio	0.519
rs45512696 – *HPN* expression raising allele (T)	44,424 / 18,032 / 1,849	16.9%	–0.002 (–0.005, 0.000) ratio	0.095
(MRI) Visceral to Gluteofemoral Fat Ratio				
HPN pLoF, AAF<1%	64,304 / 1 / 0	0.0008%	–0.155 (–0.707, 0.397) ratio	0.583
HPN pLoF plus deleterious missense (5/5 or ESM1vp), AAF<0.1%	64,188 / 117 / 0	0.091%	–0.009 (–0.060, 0.042) ratio	0.737
rs45512696 – *HPN* expression raising allele (T)	44,424 / 18,032 / 1,849	16.9%	–0.003 (–0.007, 0.001) ratio	0.115

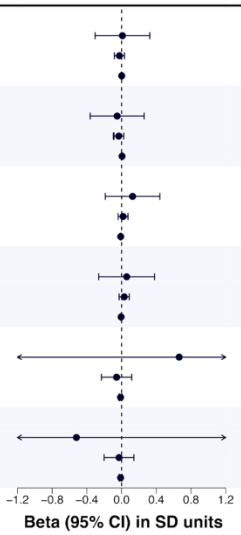

Panel b.

Outcome Gene Variant	Genotype Count RR / RA / AA	AAF	Beta (95% CI) per Allele in Clinical Units	P–Value
Body Mass Index				
HPN pLoF, AAF<1%	1,193,972 / 68 / 0	0.003%	+0.375 (–0.846, 1.596) kg/m2	0.547
HPN pLoF plus deleterious missense (5/5 or ESM1vp), AAF<0.1%	1,235,214 / 1,747 / 2	0.071%	–0.126 (–0.375, 0.123) kg/m2	0.322
rs45512696 – *HPN* expression raising allele (T)	930,575 / 280,839 / 25,495	13.4%	+0.011 (–0.009, 0.031) kg/m2	0.292
Waist to Hip Ratio (Adjusted for BMI)				
HPN pLoF, AAF<1%	591,948 / 39 / 0	0.003%	–0.002 (–0.019, 0.015) ratio	0.854
HPN pLoF plus deleterious missense (5/5 or ESM1vp), AAF<0.1%	619,844 / 1,026 / 1	0.083%	–0.001 (–0.004, 0.003) ratio	0.754
rs45512696 – *HPN* expression raising allele (T)	444,362 / 160,813 / 15,681	15.5%	+0.000 (–0.000, 0.000) ratio	0.318
HbA1c				
HPN pLoF, AAF<1%	947,295 / 53 / 0	0.003%	–0.049 (–0.293, 0.195) %	0.694
HPN pLoF plus deleterious missense (5/5 or ESM1vp), AAF<0.1%	951,157 / 1,408 / 0	0.074%	–0.000 (–0.048, 0.048) %	0.995
rs45512696 – *HPN* expression raising allele (T)	714,881 / 217,563 / 20,083	13.5%	+0.005 (0.001, 0.008) %	0.021
Random glucose				
HPN pLoF, AAF<1%	950,458 / 36 / 0	0.002%	+1.804 (–6.302, 9.910) mg/dL	0.663
HPN pLoF plus deleterious missense (5/5 or ESM1vp), AAF<0.1%	968,241 / 1,461 / 2	0.076%	–0.472 (–1.756, 0.813) mg/dL	0.471
rs45512696 – *HPN* expression raising allele (T)	708,563 / 238,389 / 22,699	14.6%	–0.085 (–0.184, 0.014) mg/dL	0.095
Liver Fat (MRI–PDFF)				
HPN pLoF, AAF<1%	63,427 / 1 / 0	0.0008%	+5.575 (–4.836, 15.985) %	0.294
HPN pLoF plus deleterious missense (5/5 or ESM1vp), AAF<0.1%	63,315 / 113 / 0	0.089%	+0.711 (–0.269, 1.691) %	0.155
rs45512696 – *HPN* expression raising allele (T)	43,832 / 17,775 / 1,821	16.9%	–0.091 (–0.169, –0.012) %	0.023
Alanine Aminotransferase				
HPN pLoF, AAF<1%	887,403 / 35 / 0	0.002%	–0.898 (–5.740, 3.944) U/L	0.716
HPN pLoF plus deleterious missense (5/5 or ESM1vp), AAF<0.1%	904,239 / 1,406 / 1	0.078%	–0.070 (–0.834, 0.693) U/L	0.857
rs45512696 – *HPN* expression raising allele (T)	656,330 / 227,190 / 22,079	15.0%	+0.046 (–0.014, 0.106) U/L	0.133
Aspartate Aminotransferase				
HPN pLoF, AAF<1%	905,525 / 35 / 0	0.002%	+1.748 (–2.386, 5.882) U/L	0.407
HPN pLoF plus deleterious missense (5/5 or ESM1vp), AAF<0.1%	922,388 / 1,427 / 1	0.077%	+0.382 (–0.262, 1.026) U/L	0.244
rs45512696 – *HPN* expression raising allele (T)	669,161 / 232,065 / 22,542	15.0%	+0.076 (0.025, 0.127) U/L	0.004
Systolic Blood Pressure				
HPN pLoF, AAF<1%	1,209,273 / 71 / 0	0.003%	–0.394 (–3.950, 3.162) mmHg	0.828
HPN pLoF plus deleterious missense (5/5 or ESM1vp), AAF<0.1%	1,250,449 / 1,789 / 2	0.072%	+0.405 (–0.325, 1.135) mmHg	0.278
rs45512696 – *HPN* expression raising allele (T)	939,887 / 286,163 / 26,133	13.5%	+0.029 (–0.028, 0.085) mmHg	0.330
Diastolic Blood Pressure				
HPN pLoF, AAF<1%	1,209,256 / 71 / 0	0.003%	–0.601 (–2.692, 1.490) mmHg	0.573
HPN pLoF plus deleterious missense (5/5 or ESM1vp), AAF<0.1%	1,250,430 / 1,789 / 2	0.072%	+0.002 (–0.428, 0.432) mmHg	0.993
rs45512696 – *HPN* expression raising allele (T)	939,874 / 286,157 / 26,133	13.5%	+0.033 (–0.000, 0.066) mmHg	0.061

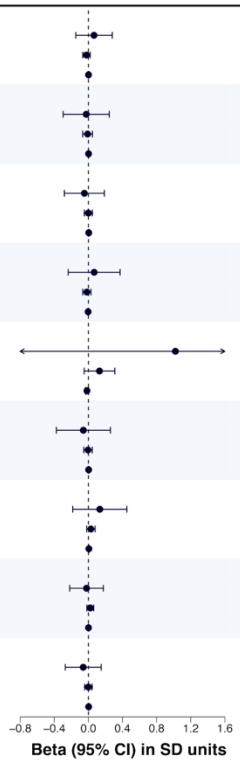

Panel c.

Outcome Gene Variant	Count (Cases) RR / RA / AA	Count (Controls) RR / RA / AA	AAF	Odds Ratio (95% CI) per Allele	P–Value
Coronary Artery Disease					
HPN pLoF, AAF<1%	81,492 / 3 / 0	608,781 / 47 / 0	0.004%	0.8 (0.2, 2.5)	0.660
HPN pLoF plus deleterious missense (5/5 or ESM1vp), AAF<0.1%	88,110 / 124 / 0	625,196 / 928 / 0	0.074%	1.0 (0.8, 1.3)	0.747
rs45512696 – *HPN* expression raising allele (T)	63,632 / 22,449 / 2,147	459,527 / 152,181 / 14,377	14.5%	1.0 (1.0, 1.0)	0.851
Myocardial Infarction					
HPN pLoF, AAF<1%	55,146 / 2 / 0	652,452 / 47 / 0	0.003%	0.8 (0.2, 2.8)	0.672
HPN pLoF plus deleterious missense (5/5 or ESM1vp), AAF<0.1%	60,896 / 84 / 0	669,874 / 985 / 1	0.073%	1.0 (0.8, 1.3)	0.941
rs45512696 – *HPN* expression raising allele (T)	44,023 / 15,469 / 1,485	492,985 / 162,549 / 15,279	14.5%	1.0 (1.0, 1.0)	0.543
Type 2 diabetes					
HPN pLoF, AAF<1%	168,794 / 13 / 0	632,058 / 37 / 0	0.003%	1.2 (0.6, 2.5)	0.655
HPN pLoF plus deleterious missense (5/5 or ESM1vp), AAF<0.1%	187,246 / 223 / 0	717,948 / 1,072 / 2	0.072%	0.9 (0.8, 1.1)	0.326
rs45512696 – *HPN* expression raising allele (T)	144,546 / 39,523 / 3,390	534,272 / 168,979 / 15,734	13.6%	1.0 (1.0, 1.0)	0.745
Liver Disease (Non Alcoholic)					
HPN pLoF, AAF<1%	45,317 / 0 / 0	632,294 / 30 / 0	0.002%	0.3 (0.1, 1.6)	0.167
HPN pLoF plus deleterious missense (5/5 or ESM1vp), AAF<0.1%	51,629 / 69 / 0	706,955 / 1,080 / 1	0.076%	0.9 (0.7, 1.2)	0.578
rs45512696 – *HPN* expression raising allele (T)	38,587 / 12,067 / 1,043	510,415 / 180,008 / 17,577	15.1%	1.0 (1.0, 1.0)	0.153
Liver Cirrhosis (Any)					
HPN pLoF, AAF<1%	12,955 / 0 / 0	646,094 / 30 / 0	0.002%	0.4 (0.0, 7.6)	0.506
HPN pLoF plus deleterious missense (5/5 or ESM1vp), AAF<0.1%	15,239 / 22 / 0	720,731 / 1,101 / 1	0.076%	1.2 (0.8, 1.8)	0.438
rs45512696 – *HPN* expression raising allele (T)	11,476 / 3,464 / 320	520,123 / 183,702 / 17,972	15.2%	1.0 (1.0, 1.0)	0.379

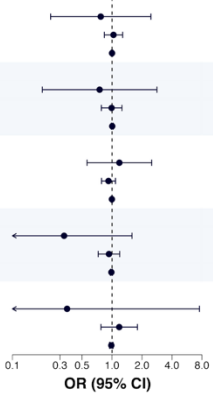

a, Associations of variants in *HPN* with anthropometric traits (Beta ± 95% CI), **b**, quantitative cardiometabolic traits (Beta ± 95% CI), and **c**, cardiometabolic outcomes (OR ± 95% CI). Association estimates are from inverse-variance weighted fixed-effect meta-analysis and *P* values are from two-sided Wald tests. AAF, alternative allele frequency; CI, confidence interval; ESM1vp, Evolutionary Scale Modeling; OR, odds ratio; pLOF, predicted loss-of-function; RR, homozygous for the reference allele; RA, heterozygous; AA, homozygous for the alternative allele.

BELIEVE Study Consortium

Recruitment Coordinators and Field Supervisors
Israt Akter, Laboni Akter, Md Shehab Uddin Al-Abid, Arnab Aditya Das, Khairul Islam, Mir Shahadul Islam, Shoriful Islam, Mohammad Kamruzzaman, Md Taslim Uddin Miah, Monalisa Moni, Sabrina Monsur, Md Mostafa Monower, K M Thouhidur Rahman, Anjuman Ara Rahman, Mantaka Rahman, A H M Rezwan, Jayashree Saha, Sharraf Samin, Kazi Nazmus Saqeeb, Monjeline Sultana, Ishrat Tasmin.

Study Site Support Workers
Md Rezaul Karim Akanda, Jesmin Akhter, Ayasha Akter, Bakul Akter, Jharna Akter, Jesmin Akter, Juba Akter, Khadiza Akter, Khadija Akter, Lipi Akter, Maksuda Akter, Mousumi Akter, Mst Lovely Akter, Nahida Akter, Nasima Akter, Samima Akter, Sema Akter, Shahida Akter, Shahnaj Akter, Shamima Akter, Taslima Akter, A T M Zorjis Alam, Mahmuda Atique, Lutfa Begum, Mst Nazma Begum, Farjana Choudhury, Md Zakir Hossain Chowdhury, Mitali Paul Chowdhury, Robin Reza Chowdhury, Mukul Rani Debnath, Kaniz Fatema, Nahid Ferdash, Naima Ferdous, Md Rakib Al Hasan, Khandaker Hashanuzzaman, Shamima Haq, Md Riazul Haque, Alamgir Hossain, Md Ibrahim, Nusrat Jahan, Shahi Israt Jahan, Israt Jahan Jarin, Zohora Pradhan Jonaki, Asik Kabir, Tonema Kader, Md Mostafa Kamal, Sayed Kamruzzaman, Sadik Fatima Kanon, Nazmul Karim, Shamsul Karim, Tanuja Khanom, Shamim Ara Khatun, Badrun Nahar Lorin, Mst Sirajum Manira, Farhana Jahan Mary, Kazi Dilruba Mita, Lipi Mitra, Basudeb Mollik, Kamrun Nahar, Sudipta Nargis, Nusrat Alam Nawmee, Esrat Zahan Nesa, Mahmuda Akter Nipa, Mehenaz Parvin, Sanjida Parvin, Shahnaj Parvin, Suraiya Parvin, Kaniz Fatema Priya, Golam Mostafa Quadrey, Nayan Rabidash, Rulia Rahman, Madhabi Rani, Shahjalal Sarker, Smriti Sarker, Razia Sultana Shathi, Fatema Shelly, Ireen Sultana, Rovaiya Sultana, Israt Jahan Sumi, Sharmin Tamanna, Khadija Akter Topy, Umme Habiba Urmee, Suraya Yesmin, Shafia Zerin.

Data Management Team
Julianne Halley, Catherine Perry, Sarah Spackman, Charlotte van Coeverden, Matthew Walker.

Laboratory Team
Mahmuda Akther Akhi, Asia Akter, Labony Akter, Ms Mili Akter, Mst Shamima Akter, Sabina Akter, Salma Akter, Setu Akter, Tahmina Akter, Md Sabdar Ali, Mst Jesmin Ara, Edyta Bujnik, Jason Crawte, Apu Chandra Das, Many Das, Samantha Farrow, Nurjahan Fatema, Md Riyad Hasan, Md Saimul Islam, Soniya Jannat, Mst Amena Khatun, Most Nurnahar Khatun, William Mossman, Robyn Murdoch, Zannaton Naeem, Danh Nguyen-Murray, Evrikleia Ntasi, Silvia Alonso Rodriguez, Most Rezina Akter Roma, Tripty Roy, Most Abida Sultana, Sharmin Akter Samia.

Study Administration Team
Nazneen Ali, Laryssa Amado, Tanya Braune, Eilidh Cowan, Steve Ellis, Ellie Farrow, Richard Houghton, Md Zahidul Islam, Giulia Loffreda, Hannah Lombardi, Ank Michielsen, Niko Ovenden, Tamara Sabri, Karen Saunders née Heasley, Md Rafiqul Islam Rabbi, Hosne Ara Rekha, Valerie Rhenius, Md Khalid Sultan, Sophie Weston, Hannah Williams.

Scientific Investigators and Collaborators

Tahmeed Ahmed, Jim Ajioka, Khondker Abdul Awal, Aytalina Azarova, Arul Baradi, Adam S Butterworth, Evangelia Chatzidiakou, Sohel Reza Choudhury, Rajiv Chowdhury, Mayank Dalakoti, John Danesh, Emanuele Di Angelantonio, Camilla Faidutti, Joerg Feldmann, Richard Fenner, Meerjady Sabrina Flora, Simon Griffin, Louise Hair, Sharifuddin Hasnat, Sarah Hawkes, Shahid Akhter Hossain, Tuhin Haque, Tafsir Hassan, Md Mominul Islam, Shafiul Islam, Maria L C Iurilli, Syed Shariful Islam, Roderic L Jones, Stephen Kaptoge, Md Khalequzzaman, Md Alfazal Khan, Kamrul Hasan Khan, Nusrat Khan, Lawrence King, Joe Lavallée, Shammi Luhar, Abdul Malik, Fazila Tun-Nesa Malik, Nick Mascie-Taylor, Md Mostafa Monower, Ruchira Tabassum Naved, Md Sirajul Islam, Aliya Naheed, Anisur Rahman, Lisa Pennells, Olalekan Popoola, Mahbubur Rahman, Rubhana Raqib, Laurie Savage, Sara Shazad, Tahmina Shirin, Lalitha Sundaram, Stephen Sutton, Henry Taylor, Aloka Tulukdar, Kim Van Daalen, Angela Wood, Luisa Zuccolo.

Fellows and Trainees
Sadika Akhter, Tanvir Chowdhury, Nurul Huda, Samia Naz Isha, Riaz Hossain Khan, Samsad Rabbani Khan, Md Mostafa Monower, Aliva Salmeen, Zeeba Zahra Sultana, Animesh Talukder, Renesa Tarannum.

External Advisory Board (CAPABLE Initiative)
Colin Baigent (Chair), Abbas Bhuiya, Shahida ‘Lucky’ Parvin.

Steering Committee & Data and Sample Access Committee (current membership)
Sohel Reza Choudhury, John Danesh, Emanuele Di Angelantonio, Simon Griffin, Md Khalequzzaman, Md Alfazal Khan, Nick Mascie-Taylor.

References

1 Taliun, D. *et al.* Sequencing of 53,831 diverse genomes from the NHLBI TOPMed Program. *Nature* **590**, 290-299 (2021). https://doi.org/10.1038/s41586-021-03205-y

2 Mbatchou, J. *et al.* Computationally efficient whole-genome regression for quantitative and binary traits. *Nat Genet* **53**, 1097-1103 (2021). https://doi.org/10.1038/s41588-021-00870-7

3 Loh, P. R., Kichaev, G., Gazal, S., Schoech, A. P. & Price, A. L. Mixed-model association for biobank-scale datasets. *Nat Genet* **50**, 906-908 (2018). https://doi.org/10.1038/s41588-018-0144-6

4 Yengo, L. *et al.* A saturated map of common genetic variants associated with human height. *Nature* **610**, 704-712 (2022). https://doi.org/10.1038/s41586-022-05275-y

5 Wang, G., Sarkar, A., Carbonetto, P. & Stephens, M. A simple new approach to variable selection in regression, with application to genetic fine mapping. *J R Stat Soc Series B Stat Methodol* **82**, 1273-1300 (2020). https://doi.org/10.1111/rssb.12388

6 Hindy, G. *et al.* Rare coding variants in 35 genes associate with circulating lipid levels-A multi-ancestry analysis of 170,000 exomes. *Am J Hum Genet* **109**, 81-96 (2022). https://doi.org/10.1016/j.ajhg.2021.11.021

7 Liu, D. J. *et al.* Exome-wide association study of plasma lipids in >300,000 individuals. *Nat Genet* **49**, 1758-1766 (2017). https://doi.org/10.1038/ng.3977

8 Shungin, D. *et al.* New genetic loci link adipose and insulin biology to body fat distribution. *Nature* **518**, 187-196 (2015). https://doi.org/10.1038/nature14132

9 Akbari, P. *et al.* Multiancestry exome sequencing reveals INHBE mutations associated with favorable fat distribution and protection from diabetes. *Nat Commun* **13**, 4844 (2022). https://doi.org/10.1038/s41467-022-32398-7

10 Pers, T. H. *et al.* Biological interpretation of genome-wide association studies using predicted gene functions. *Nat Commun* **6**, 5890 (2015). https://doi.org/10.1038/ncomms6890

11 Niehues, T. *et al.* Mutations of the gene FNIP1 associated with a syndromic autosomal recessive immunodeficiency with cardiomyopathy and pre-excitation syndrome. *Eur J Immunol* **50**, 1078-1080 (2020). https://doi.org/10.1002/eji.201948504

12 Saettini, F. *et al.* Absent B cells, agammaglobulinemia, and hypertrophic cardiomyopathy in folliculin-interacting protein 1 deficiency. *Blood* **137**, 493-499 (2021). https://doi.org/10.1182/blood.2020006441

13 Roncareggi, S., Iritani, B. M. & Saettini, F. FNIP1 Deficiency: Pathophysiology and Clinical Manifestations of a Rare Syndromic Primary Immunodeficiency. *Curr Issues Mol Biol* **47** (2025). https://doi.org/10.3390/cimb47040290

14 Sattler, E. C. & Steinlein, O. K. in *GeneReviews((R))* (eds M. P. Adam *et al.*) (1993).

15 Custode, B. M. *et al.* Folliculin depletion results in liver cell damage and cholangiocarcinoma through MiT/TFE activation. *Cell Death Differ* **32**, 1460-1472 (2025). https://doi.org/10.1038/s41418-025-01486-8